High-statistics measurement of g_a/g_v in $\Lambda \rightarrow p + e^- + \bar{\nu}$

J. Dworkin,[a] P. T. Cox,[b] E. C. Dukes,[c] and O. E. Overseth
Department of Physics, University of Michigan, Ann Arbor, Michigan 48109

R. Handler, R. Grobel,[d] B. Lundberg,[e] L. Pondrom, M. Sheaff, and C. Wilkinson[f]
Department of Physics, University of Wisconsin, Madison, Wisconsin 53706

A. Beretvas,[e] L. Deck,[g] T. Devlin, K. B. Luk,[h] and R. Rameika[e]
Department of Physics, Rutgers, The State University, Piscataway, New Jersey 08854

K. Heller
School of Physics and Astronomy, University of Minnesota, Minneapolis, Minnesota 55455
(Received 28 April 1989)

The analysis of 37 286 Λ β decays yields the axial-vector-to-vector coupling ratio $g_a(0)/g_v(0) = +0.731 \pm 0.016$, $\alpha_{ev} = -0.27 \pm 0.013$ with the weak-magnetism coupling $w = g_w(0)/g_v(0) = 0.15 \pm 0.30$. The error is statistical only and there is no evidence for any significant systematic error. A new method is presented for resolving problems arising from the quadratic ambiguity in the analysis of this decay process. The q^2 dependence of the form factors has been included. Both the internal and external radiative corrections have been made. If w is constrained to be 0.97, the conserved-vector-current value, $g_a(0)/g_v(0) = +0.719 \pm 0.016 \pm 0.012$, where the uncertainties are statistical and systematic, respectively. The corresponding value of the electron-neutrino correlation is $\alpha_{ev} = -0.017 \pm 0.013 \pm 0.010$.

I. INTRODUCTION

A. Theoretical background

Much of the information on baryon semileptonic decays is based on low-statistics experiments. The strangeness-changing Λ β decay

$$\Lambda \rightarrow p + e^- + \bar{\nu}$$

has been measured a number of times,[1-6] but only relatively recently with high statistics by Wise *et al.*[7] [10 000 events, $|g_a(0)/g_v(0)| = 0.734 \pm 0.031$] and Bourquin *et al.*[8] [7111 events, $g_a(0)/g_v(0) = +0.70 \pm 0.03$]. In this paper we present an analysis of 37 286 Λ β decays obtained in an experiment performed in the neutral-hyperon beam at Fermilab. These data were used to extract a more precise measurement of the ratio of axial-vector to vector weak coupling constants as a test of the standard model of flavor-changing weak decays.[9]

The matrix element for the decay is

$$M = (G/\sqrt{2}) \langle p | J^\mu | \Lambda \rangle \overline{u_e}(p_e) \gamma_\mu (1+\gamma_5) u_\nu(p_\nu) , \quad (1.1)$$

where G is the universal weak coupling constant, and the leptonic current has the standard $V-A$ form. The hadronic part is[10]

$$\langle p | J^\mu | \Lambda \rangle = \overline{u_p} [g_v(q^2) \gamma^\mu + g_w(q^2) \sigma^{\mu\nu} q_\nu M_\Lambda + g_a(q^2) \gamma^\mu \gamma_5 + g_2(q^2) \sigma^{\mu\nu} q_\nu \gamma_5 / M_\Lambda] u_\Lambda \sin(\theta_C) , \quad (1.2)$$

where θ_C is the Cabibbo angle, q^2 is the four-momentum transfer squared, g_v is the vector coupling, g_a is the axial-vector coupling. g_w is the weak-magnetism term, and g_2 is the second-class-current term which we will take to be zero. We have neglected terms of order M_e^2/M_Λ^2. We make the usual assumption of the q^2 dependence of the form factors as follows:

$$g_v(q^2) = g_v(0)[1 + 2(q/M_v)^2] ,$$

$$g_a(q^2) = g_a(0)[1 + 2(q/M_a)^2] ,$$

$$g_w(q^2) = g_w(0) ,$$

where $M_v = 0.97$ GeV/c^2, $M_a = 1.25$ GeV/c^2 (Ref. 11). The weak-magnetism term is assumed to have no q^2 dependence. The expression for the differential decay rate can then be factored into a term which depends only on the kinematics of the decay, W, and a term T. This term T depends on the ratio of the vector and axial-vector coupling constants, and also on the ratio of the weak-magnetism and axial-vector coupling constants. The explicit expressions for W and T are given in Appendix A (Ref. 12). We have

$$d^2\Gamma/dE_e^* d(\cos\theta_{e\nu}^*) = W(E_e^*, \cos\theta_{e\nu}^*) \times T(E_e^*, \cos\theta_{e\nu}^*, g_a(0)/g_v(0), g_w/g_v(0)) , \quad (1.3)$$

where E_e^* is the electron energy in the Λ rest frame, and $\cos\theta_{e\nu}^*$ is the cosine of the angle between the electron and the neutrino in the Λ rest frame. The value of the weak-

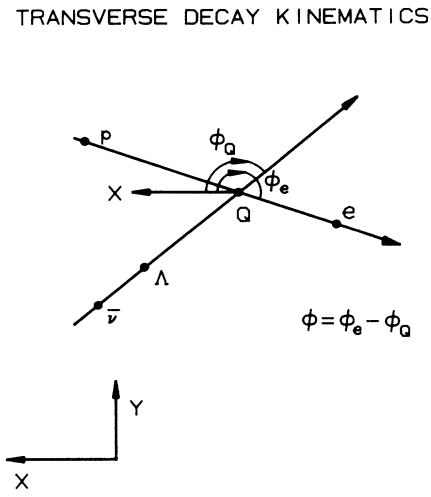

FIG. 1. This figure gives the transverse decay kinematics for $\Lambda \to p e^- \bar{\nu}$. The decay sequence is $\Lambda \to Q + \bar{\nu}$ and $Q \to p + e^-$. In the laboratory system consider a plane perpendicular to the Λ momenta, and place a dot where the trajectory of the electron, proton, Q particle, Λ, and neutrino intersect this plane. Measure the angles Φ_Q and Φ_e clockwise from an axis through Q parallel to the laboratory x axis (as shown in the figure). The angle Φ is defined to be $\Phi_e - \Phi_Q$. All vectors and all angles are in the plane of the figure.

magnetism term $g_w/g_v(0)$ is usually given by the conserved-vector-current hypothesis:

$$g_w/g_v(0) = (\mu_p - 1) g_v(0) M_\Lambda / (M_p + M_\Lambda) = 0.97 \ ,$$

where μ_p is the proton magnetic moment expressed in Bohr magnetons. However this need not be the case, a short discussion of another hypothesis is given in Sec. V D.

B. Overview of data analysis

Four particles are involved in the decay $\Lambda \to p e^- \bar{\nu}$. The p and e^- are fully reconstructed by our magnetic spectrometer, the direction but not the magnitude of the Λ momentum is known and the $\bar{\nu}$ is not observed. In the center-of-mass system there are two solutions for the magnitude of the Λ momentum.

Two different methods were used to extract $g_a(0)/g_v(0)$. The first, more standard approach used the distribution of events in the variable $\cos\theta^*_{ev}$. There are two solutions for $\cos\theta^*_{ev}$ which reflects the lack of knowledge of the longitudinal component of the $\bar{\nu}$ momentum in the Λ rest frame. The two solutions correspond to different Λ momenta in the laboratory. We have measured the Λ momentum spectra by using the $\Lambda \to p\pi^-$ decays and have weighted the two solutions by their probabilities as given by that spectrum. A second

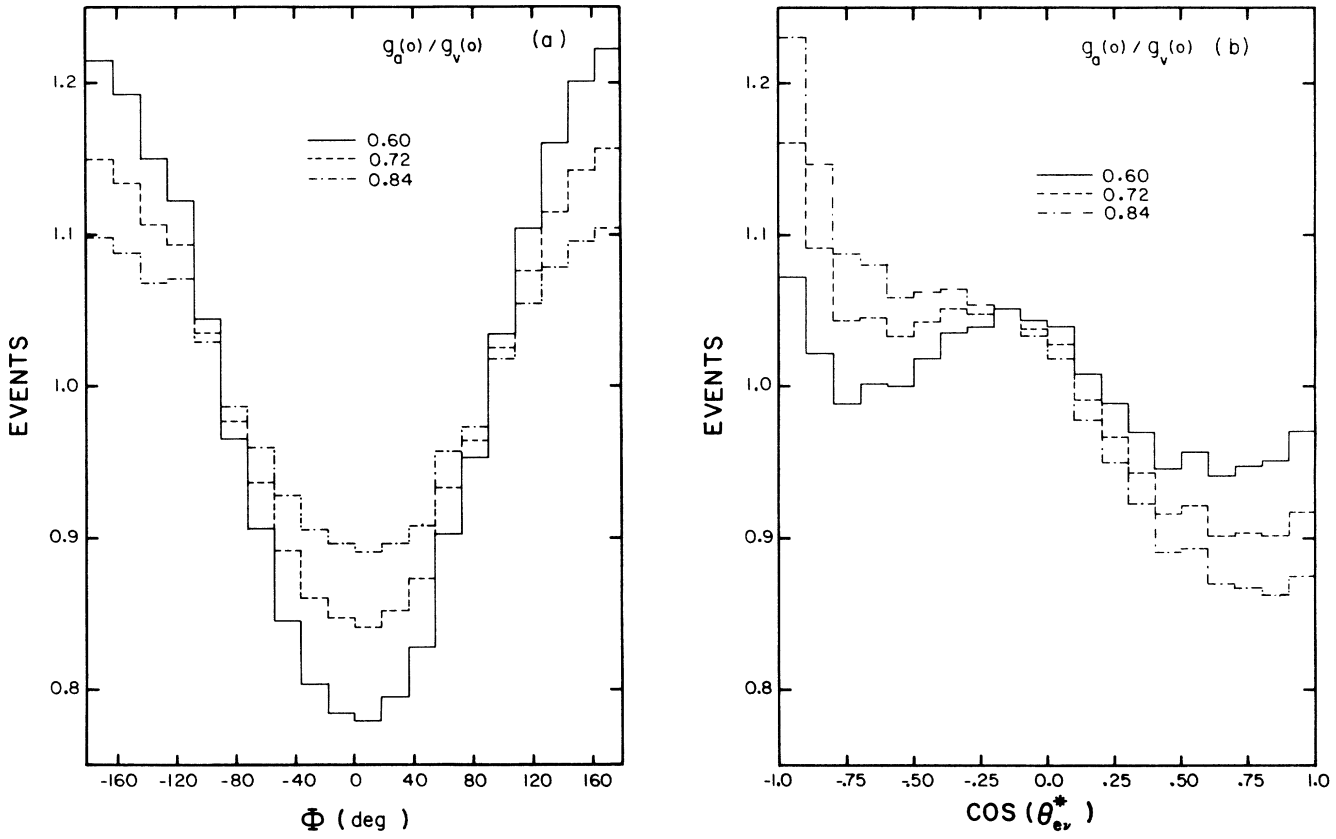

FIG. 2. (a) The Monte Carlo Φ distribution is plotted for three values of $g_a(0)/g_v(0)$ (0.60, 0.72, and 0.84). The average value for a bin has been normalized to 1. The size of a bin is 18 degrees. The number of events in the Monte Carlo sample is 10 times the data sample (37 286). (b) The Monte Carlo $\cos(\theta^*_{ev})$ distribution is plotted for the same three values of $g_a(0)/g_v(0)$ and uses the same normalization. The size of each bin is 0.1.

method is free of the problem of the kinematic ambiguity, and gives a slightly more precise answer. Because the direction of the Λ is known, and the momentum of the proton and electron are measured, the momentum of each daughter particle perpendicular to the direction of the Λ can be determined. Although the momentum of $\bar{\nu}$ has two values, its transverse momentum is uniquely determined by conservation of momentum, $\mathbf{P}_{p\perp}+\mathbf{P}_{e\perp}+\mathbf{P}_{\nu\perp}=0$. This observation leads us to consider angular variables in a plane transverse to the Λ direction in order to extract $g_a(0)/g_v(0)$.

We consider, for purposes of analysis, the decay sequence

$$\Lambda \rightarrow Q+\bar{\nu}, \quad Q \rightarrow p+e^- ,$$

where Q is a fictitious particle with a wide mass distribution. In the laboratory system consider a plane P perpendicular to the direction of the neutral beam. The plane is illustrated in Fig. 1. By momentum conservation, the points where the particles p, Q, and e^- intersect this plane lie on a straight line. For the same reason the points where Λ, Q, and $\bar{\nu}$ intersect this plane also lie on a straight line. Since there is no twofold kinematic ambiguity in this plane, the distribution of the angle Φ between these two lines is more sensitive to $g_a(0)/g_v(0)$ than the distribution of $\cos\theta^*_{ev}$. This is illustrated in Fig. 2(a) which shows how the Φ distribution differs for three values of $g_a(0)/g_v(0)$ as determined by our Monte Carlo program. Figure 2(b) shows the same comparison for $\cos\theta^*_{ev}$.

II. EXPERIMENTAL TECHNIQUE

A. Spectrometer

A detailed discussion of the experimental equipment can be found in Ref. 13. The salient features will be reviewed here. The apparatus and coordinate system are shown in Fig. 3. The 400-GeV proton beam produced Λ hyperons in a 3-mm-diameter Be target. A 4-mm-diameter collimator embedded in the vertical (y) magnetic field of 2.3 Tesla ($M2$) determined the Λ direction. Λ hyperons were detected by observing their charged decay products in a magnetic spectrometer downstream of the evacuated decay region. Their characteristic neutral vee decay topology, which consisted of two oppositely charged particles emanating from a single point in the decay region, is illustrated in Fig. 3. Two sets of three multiwire proportional chambers (MWPC's) $C1$–$C6$ with a 2-mm signal-wire spacing, each with two orthogonal signal planes, measured the track coordinates upstream and downstream of the 60-cm (horizontal)×20-cm (vertical)×190-cm (long) aperture dipole magnet ($M3$). The same neutral vee signature was typical of the dominant decay mode $\Lambda \rightarrow p\pi^-$ which was 1300 times more frequent than the β decay and the major source of background. To suppress this background two different types of electron identification were used.

B. Electron identification

Electrons and pions emit vastly different amounts of synchrotron radiation when bent in the 3.13-T m spectrometer magnet $M3$. These synchrotron x rays were detected by a xenon-filled multiwire proportional chamber (SRD) immediately downstream of $M3$ (Ref. 14). The amount of synchrotron radiation emitted by a particle per unit length in a uniform magnetic field varies as E^2/M^4. The x rays gave a characteristic hit pattern in this chamber which distinguish the electrons from the more massive pions. After passing through the xenon chamber, the electron was intercepted by a lead-glass array (see Fig. 4) located downstream of $C5$. The array contained a total of 25 radiation lengths (r.l.), sampling the electromagnetic shower development every 3.1 r.l. (Ref. 13). Electron candidates were required to have a longitudinal shower development consistent with an elec-

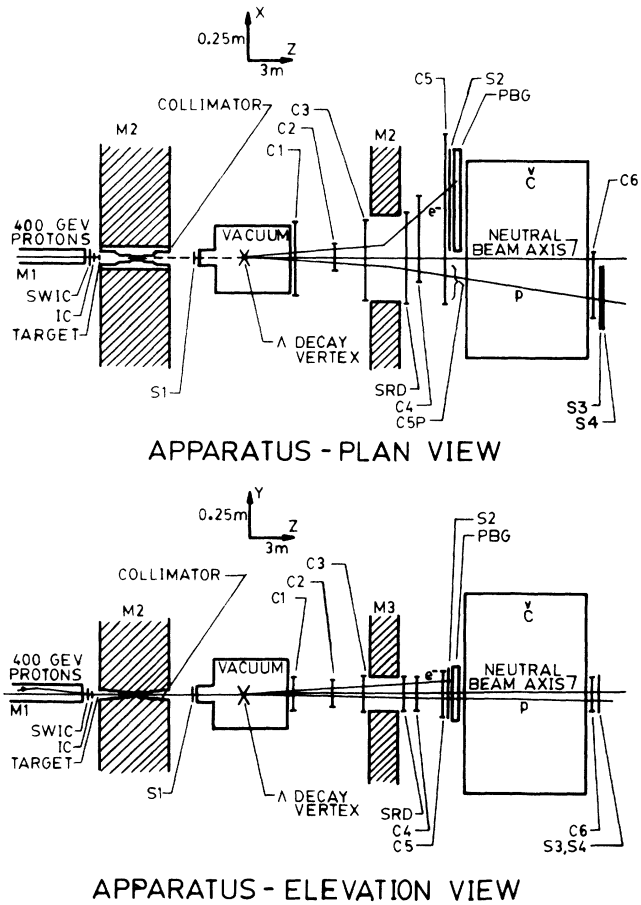

FIG. 3. The plane and elevation views of the experimental apparatus. The synchrotron-radiation detector (SRD) was immediately downstream of the analysis magnet. The S's denote scintillation counters, the C's refer to argon-filled multiwire proportional chambers in the magnetic spectrometer, and C refers to the Cherenkov counter. PBG is the lead-glass array. A Λ β-decay event is illustrated.

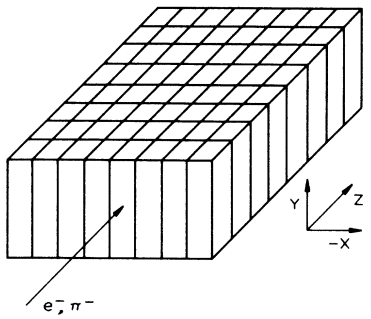

FIG. 4. The lead-glass array consists of 64 lead-glass blocks, each 10 cm×10 cm×39 cm, which were arranged with their long axes vertical. The array was eight blocks wide and eight blocks deep.

tromagnetic shower and a total deposited energy equal to the momentum determined by the spectrometer.

C. Proton identification

It was necessary to distinguish other background processes characterized by the neutral vee topology where one of the decay products was an electron, such as kaon decay $K_L \to \pi^+ e^- \bar{\nu}$ (K_{e3}), or pair production ($\gamma \to e^+ e^-$) in the small amount (0.02 r.l.) of material present in the decay region. These processes, while less likely than $\Lambda \to p\pi^-$ events, competed with the rare $\Lambda \to p e^- \bar{\nu}$ mode (see Table I). Protons were distinguished from higher-velocity positrons and positively charged pions with a 0.06-atm air-filled threshold Cherenkov counter located between $C5$ and $C6$. Further identification and rejection of positrons was achieved with a 2-r.l. lead radiator-scintillator ($E1 = S3 \cdot \overline{S4}$) combination downstream of $C6$. Off-line rejection of positrons was possible because the positrons produced a larger pulse height in the scintillator $S4$ than did protons.

TABLE I. Typical rates for electronic trigger and reconstructed events.

Triggers per accelerator pulse	
V	7500
$V \cdot$glass	1100
$V \cdot \bar{C} \cdot$glass	600
Λ_β	75
Reconstructed events (no prescale factor)	
$\Lambda \to p\pi^-$	3750
$K_S \to \pi^+\pi^-$	700
$\gamma \to e^+ e^-$	250
$K_L \to \pi^+ e^- \nu$	15
Λ_β	0.6

D. Trigger

The trigger that selected $\Lambda \to p e^- \bar{\nu}$ decays ($\Lambda\ \beta$ decays) used the threshold Cherenkov counter and both electron detectors to supplement the requirement that a neutral vee decay topology had been detected. The trigger logic is given in Fig. 5. It was implemented in two stages.

In the first stage the coincidence $V = \overline{S1} \cdot C1 \cdot C5P \cdot S2 \cdot C6 \cdot S3$ was formed using prompt signals from the spectrometer MWPC's and scintillation counters. It required two oppositely charged particles to originate in the decay region between $S1$ and $C1$, yielding a high concentration (50%) of reconstructable $\Lambda \to p\pi^-$ decays. $S2$ was used to determine that a negative particle entered the lead-glass array while $S3$ ensured that the positive particle had a high momentum characteristic of a proton from Λ decay.

In parallel with this V trigger, a signal from the lead-glass array, ES, was produced by logic which required a minimum energy deposition of 6 GeV in the initial 12.4 r.l. of the array. If a deposition of energy greater than 1 GeV occurred in the final 6.2 r.l. of the array the signal ES was produced only if at least 11 GeV was deposited in the initial part of the array. In this trigger, the lead glass had an efficiency of 98% for electrons with a hadron re-

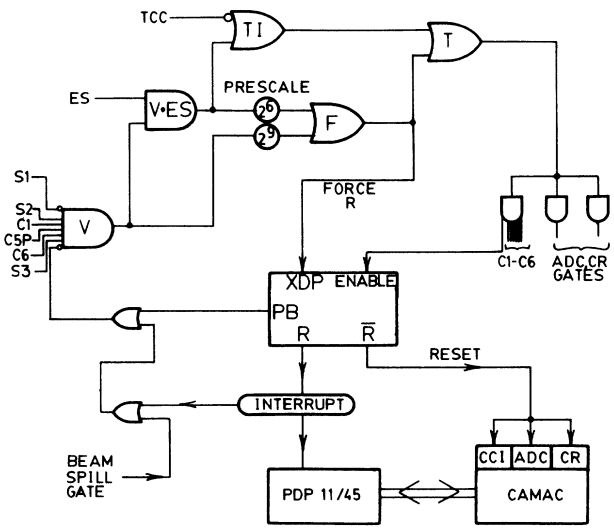

FIG. 5. Shown are the trigger logic and data acquisition system. The trigger has two parts: a fast trigger and a slow trigger (xenon data processor, denoted XDP). The fast trigger consisted of a V trigger, the V in coincidence with the lead glass (ES), and the $V \cdot$ES in anticoincidence with the threshold Cherenkov counter (TCC). The V trigger was gated off during the operation of the processor by a busy signal, denoted PB. A decision was made in 16 μsec. A positive response, denoted R, was generated by the processor when the requirements of the synchrotron radiation trigger were satisfied by the event.

jection factor of 7. These signals were combined with the absence of a Cherenkov-counter signal (TCC) to form the coincidence $\beta = V \cdot \overline{\text{TCC}} \cdot \text{ES}$. When β occurred the MWPC hits were stored, the electronics were gated off, and the second stage of the trigger was started. This stage consisted of an electronic device which processed the xenon chamber data and, in 16 μsec, decided if an electron candidate were present. A negative decision caused a reset pulse to be sent to the chamber readout latches and then released the electronics for another event. A positive decision (SR) caused the data to be read out.[14] The total trigger is denoted by $\text{LB} = \beta \cdot \text{SR}$. The efficiency of the synchrotron radiation detector for triggering on electrons was 82% with a hadron rejection factor of 17.

The PDP 11/CAMAC data-acquisition system was triggered by two other logic signals, each reduced electronically by a numerical factor and mixed with LB. A prescaling factor of $\frac{1}{512}$ for the V triggers provided a sample of $\Lambda \to p\pi^-$ for normalization and calibration purposes. The small concentration (4%) of reconstructed e^+e^- pairs obtained with the V trigger was increased to 19% by the coincidence $V \cdot \text{ES}$ reduced by a factor of $\frac{1}{64}$ to provide a sample of momentum-analyzed electrons used to monitor the performance of the electron detectors.

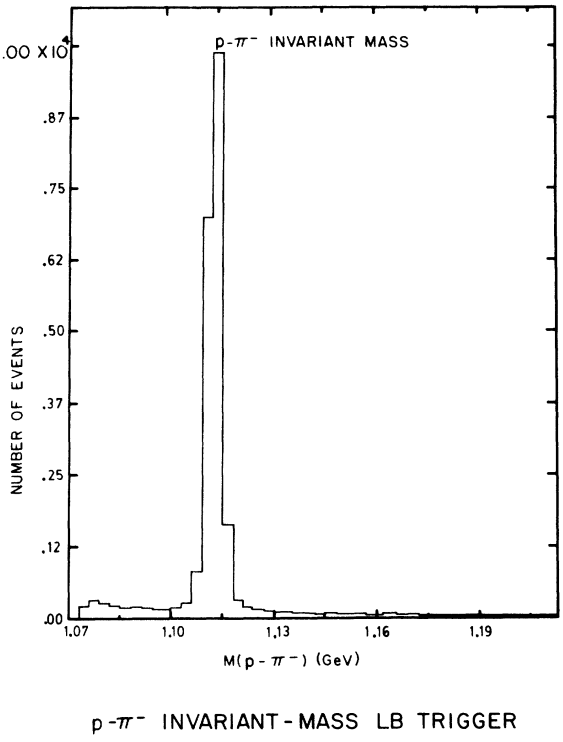

FIG. 6. The invariant mass ($p\pi^-$) of the Λ β-decay triggers. The size of each bin is 0.003 GeV.

III. SELECTION OF THE FINAL-EVENT SAMPLE

A. V topology

The MWPC data were used by the pattern recognition software to reconstruct the neutral vee topology and calculate the deflection angle of the charged decay products in $M3$. One-half of the Λ β-decay triggers yielded well-reconstructed vees, providing a sample of 3.4×10^6 events. The calculated p-π^- invariant mass for these Λ β-decay candidates shows a large Λ peak illustrating the nonleptonic background which must be rejected off-line (see Fig. 6). The vee reconstruction efficiency was determined by a Monte Carlo simulation to be 96%. Cuts applied to the reconstructed vees required that the reconstructed tracks be well within the real spectrometer apertures, have a decay vertex inside the decay region, and have a momentum ratio (p_+/p_-) greater than 2.4 (the minimum for $\Lambda \to p e^- \bar{\nu}$). Using these cuts and additional off-line electron identification cuts (discussed in Sec. III B below) the β-decay signal is further enhanced as shown in Fig. 7, and the number of β-decay candidates has been reduced to 98 736. By using the cuts listed in Table II the final $\Lambda \to p e^- \bar{\nu}$ decay sample of 37 286 was obtained. Table II lists all cuts in the order they were imposed and shows the transmission of each for real and Monte Carlo events. The first cut in Table II is that the sum of the momentum of the charged particles was required to be less than 380 GeV/c. We also eliminated a possible confusion between electron and proton tracks by requiring an adequate separation (more than 2 mm at $C5$) in the vertical view [Table II (2)]. In addition we cut events which had no detectable separation of the tracks

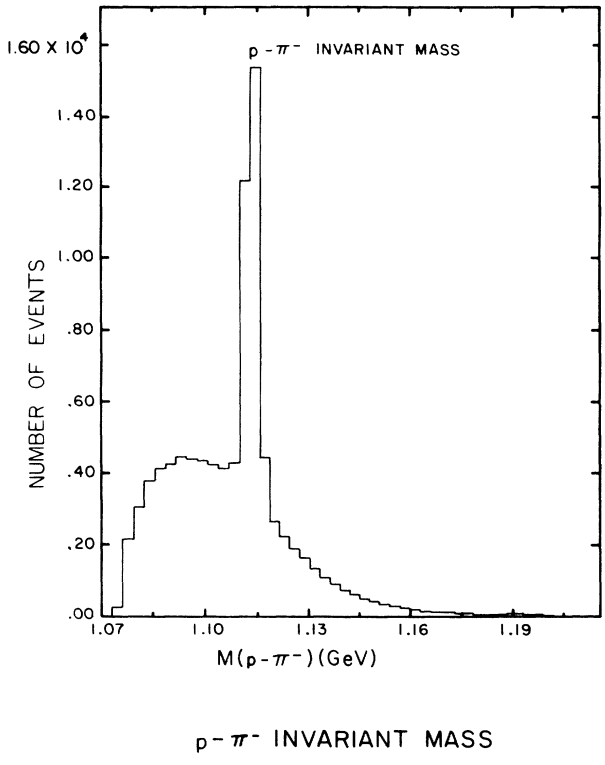

FIG. 7. The invariant mass ($p\pi^-$) after the off-line requirements had been satisfied for both the lead glass and the synchrotron detector. The size of each bin is 0.003 GeV.

TABLE II. Event selection.

		Data	Monte Carlo events
		98 736	853 113
(1)	$\lvert P_{ex}+P_{pz}\rvert < 380$ GeV/c	98 708	853 113
(2)	$\lvert y_e - y_p\rvert > 2$ mm	97 816	838 155
(3)	$\gamma \to e^+e^-$	97 575	821 686
(4)	Collimator circle	94 737	802 872
(5)	Kinematic circle	90 437	789 874
(6)	Ellipse in the target plane (see Fig. 19)	45 330	511 830
(7)	$\theta_Q > 600$ μrad for $M = M_{p\pi^-}$	40 692	477 454
(8)	y at spectrometer exit	40 257	473 186
(9)	Electron x at spectrometer exist	40 186	473 164
(10)	Electron y at lead glass	40 082	445 705
(11)	Proton x at back counter	40 078	394 582
(12)	$\lvert \tilde{p}_{e\parallel}/\tilde{p}_e\rvert \leq 0.95$	37 286	372 860

upstream of the analysis magnet [$\gamma \to e^+e^-$ topology Table II (3)].

B. Off-line electron identification

Off-line electron signature requirements from the lead-glass array, which measured the energy E_e of an incident electron with a resolution $\sigma(E_e)/E_e = 0.20/\sqrt{E_e}$, included a momentum-dependent requirement that the total energy deposited be at least 87% of the incident momentum measured by the magnetic spectrometer. At least 15% of the total energy was required to be present in the first 6.2 r.l. A hadron rejection factor of 145 was achieved with an electron efficiency of 95%. The off-line electron signature from the synchrotron radiation detector required that at least one synchrotron x-ray photon had been detected, achieving an additional hadron rejection factor of 30 (Ref. 14).

C. Target-pointing requirements

The events, which satisfied the electron requirements and cuts described earlier, were examined to see if they were consistent with the geometry of our beam-defining collimator and production target and with $\Lambda \to Q + \bar{\nu}$ kinematics. The consistency of these three conditions is given geometrically as the intersection region of three circles as shown in Fig. 8 [Table II(4) and II(5)], and described in the following paragraph.

The condition that the parent Λ be produced in the Be target (B), and pass through the collimator (C), is equivalent to demanding that the reconstructed production point $\Lambda = (x_\Lambda, y_\Lambda, z_T)$ be inside a 3-mm-diameter circle on the target plane centered at the position (x_B, y_B). In addition the production point must be inside a circle which is the image of the collimator (C) at the target plane for a point source at the reconstructed decay point z_d. A third circle is determined by the kinematics (K). After the event is reconstructed, the mass and momentum of the fictitious particle Q is known. For an event to be consistent with the decay hypothesis $\Lambda \to Q + \bar{\nu}$, the momentum of the Q in the Λ center of mass must be $p_Q^* = [(M_\Lambda)^2 - (M_Q)^2]/2M_\Lambda$ and the transverse momentum in that frame is

$$p_{Q\perp}^* = p_Q^* \sin\theta_{\Lambda Q}^* < [(M_\Lambda)^2 - (M_Q)^2]/2M_\Lambda ,$$

where $\theta_{\Lambda Q}^*$ is the center-of-mass angle between $\mathbf{p}_Q^*$ and

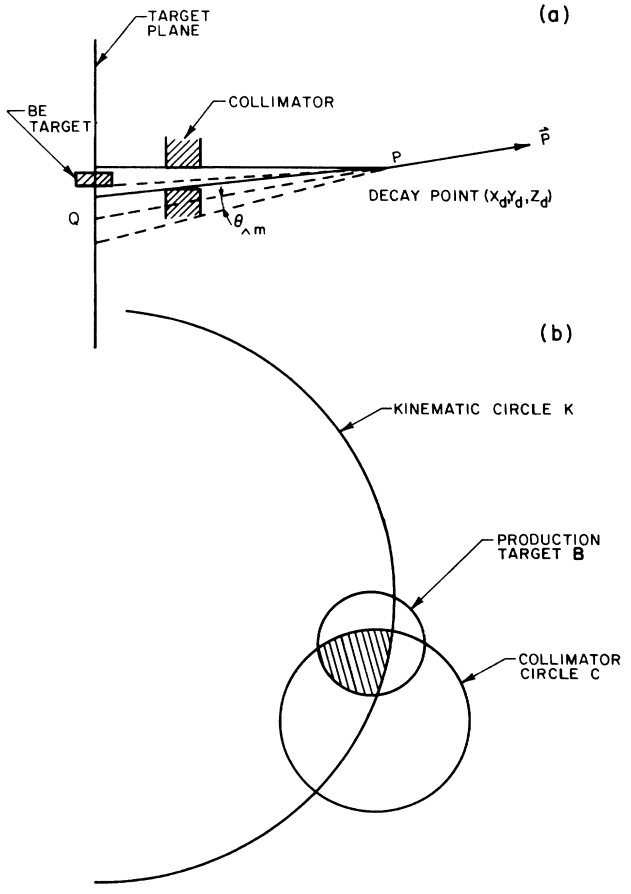

FIG. 8. This figure illustrates three circles: the production target circle B, the collimator circle C, and the kinematic circle K.

the Λ direction in the laboratory. Transforming to the laboratory system $p_{Q\perp}=p^*_{Q\perp}$ and

$$\theta_{\Lambda Q} < [(M_\Lambda)^2-(M_Q)^2]/2M_\Lambda p_Q \ ,$$

where $\theta_{\Lambda Q}$ and p_Q are in the laboratory. Thus the Λ vector has to be inside a cone whose axis is p_Q, vertex is at z_d and opening angle is

$$\theta_{\Lambda Q}=[(M_\Lambda)^2-(M_Q)^2]/2M_\Lambda p_Q \ .$$

The vector $\mathbf{p}_Q$ intersects the target plane at (x_Q,y_Q) and all events must be within a circle centered on this point with a radius of $(z_d-z_B)\theta_{\Lambda m}$. Figure 8 shows these circles for a typical event. The cross-hatched region shows the allowable locations for the production point Λ. For such an event the position of Λ at production is assigned at the mean position of the allowable region.

One cannot eliminate all events which do not pass the three-circle test (events for which B, C, and K have no common interior points). Measuring errors can move the decay vertex (x_d,y_d,z_d) enough to cause the data from a valid β decay to fail this test. If it is possible to pick a new decay point $(x_d+\delta x,y_d+\delta y,z_d+\delta z)$ in such a way that the event will pass the three-circle test and still fit the event topology as determined by the ratio of δx, δy, and δz to their expected errors, the decay vertex for the event was so modified and the event was retained. If not, the event was cut. In order to reduce further the $\Lambda\rightarrow p+\pi^-$ background, any event whose $p\pi^-$ mass was within three standard deviations of M_Λ was required to have $\theta_{\Lambda Q}>0.6$ mrad.

D. Monte Carlo program

To analyze the data a Monte Carlo program was written in which events were generated according to the expected differential decay rate. For each real event ten Monte Carlo events were generated. The Λ laboratory energies were picked to be consistent with the Λ spectrum as measured by the $\Lambda\rightarrow p\pi^-$ events, and the longitudinal coordinate of the decay point z_d was chosen consistent with the Λ lifetime ($c\tau=7.89$ cm) (Ref. 15). The Λ direction was picked by choosing random points on its trajectory at the production target and defining collimator aperture. The target center (x_B,y_B) and the collimator center (x_C,y_C) were found using measured $\Lambda\rightarrow p\pi^-$ decays. The electron energy and the neutrino energy were chosen at random consistent with a Dalitz-plot probability distribution for unpolarized Λ's for a given value of $g_a(0)/g_v(0)$. This determines $\cos\theta^*_{ev}$. The other randomly chosen variables were the three angles determining the orientation of the decay plane in the Λ center of mass. The angles in the Monte Carlo event, transformed into the laboratory, were varied by angular uncertainties appropriate to the measurement errors of the real events. These generated events were subjected to exactly the same selection criteria (summarized in Table II) as the data.

The Monte Carlo program was not a detailed simulation of the apparatus but was designed to determine the effects of apertures and data selection criteria on the relevant angular distributions, Φ and $\cos\theta^*_{ev}$. Nevertheless, the agreement between Monte Carlo simulation and the particle distributions in the spectrometer is good, as seen in Figs. 9–15. The x, y, and z distributions of the decay vertex are given in Fig. 10. The electron distribution at the exit of the spectrometer magnet is given in Fig. 11. The center part of the distribution has been depleted because very forward electrons ($\cos\tilde{\theta}_e>0.95$) have been cut. The proton position at chamber 6 is given in Fig. 12. The discrepancy at $x=-17$ cm has been investigated by forcing agreement between data and Monte Carlo simulation with no statistically significant change in the answer for $g_a(0)/g_v(0)$. This illustrates the general feature that our analysis depends on variables which are only indirectly correlated to the fixed laboratory coordinates and as such are relatively insensitive to the details of apparatus response. The energy of the neutrino in the Λ rest frame is given in Fig. 13.

E. Background rejection

The electron and proton laboratory energies are given in Figs. 14 and 15. The invariant-mass plot for the $p\pi^-$-hypothesis for the final data sample is given in Fig. 9.

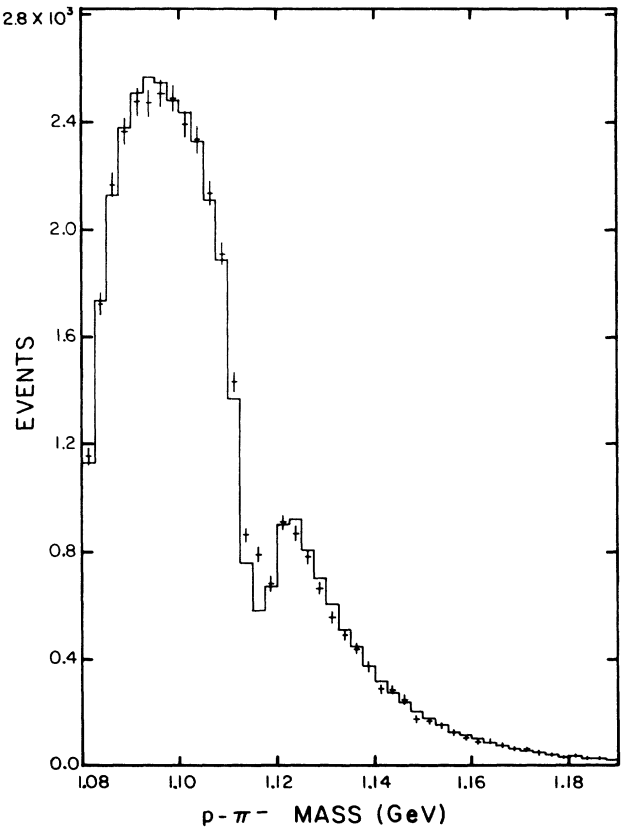

FIG. 9. The invariant mass ($p\pi^-$) for the final Λ β-decay sample. The size of each bin is 0.0025 GeV. The data points are shown with error bars; the solid line is a Monte Carlo simulation.

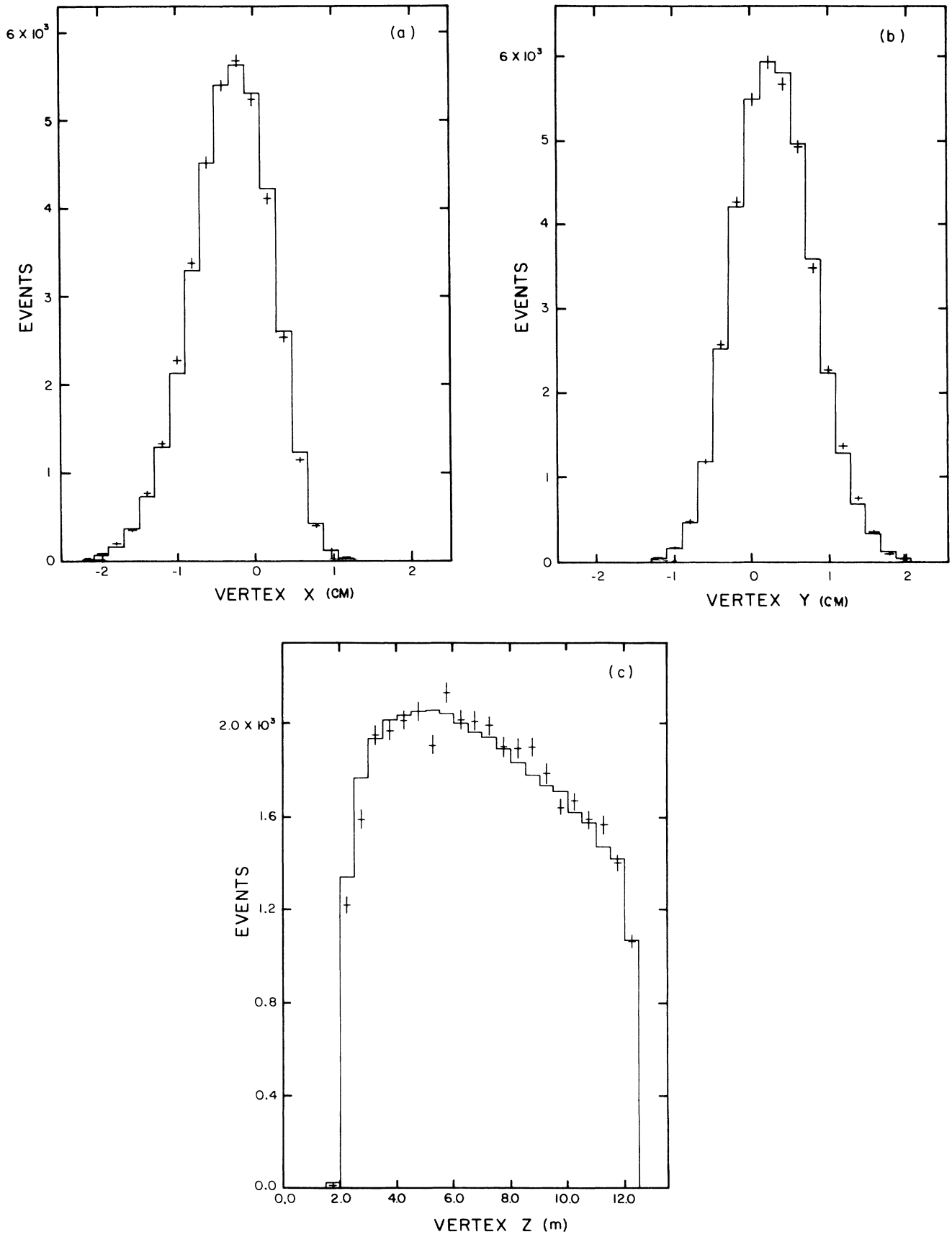

FIG. 10. (a) The x, (b) y, and (c) z vertex distributions. The sizes of the bins are 2 mm, 2 mm, and 0.5 m, respectively. This figure refers to the final Λ β-decay sample. The data points are shown with error bars; the solid line is a Monte Carlo simulation.

The discrepancy in the region of the Λ mass is due to contamination by $\Lambda \to p\pi^-$ events. From Fig. 9 this contamination is estimated to be 0.6% of the Λ β-decay sample. The fraction of background $\Lambda \to p\pi^-$ events that is outside the Λ mass region is determined by analyzing an enriched $\Lambda \to p\pi^-$ sample, the V trigger events, which pass all the cuts (see Table II) used in the Λ β-decay analysis. For these V trigger events the π^- were subjected to the electron cuts. This analysis indicates that there are approximately twice as many $p\pi^-$ events outside the Λ mass region after cuts as in it, resulting in a background of 1.7%. When the Φ distribution corresponding to the 1.7% of the V triggers that pass all the cuts is added to the normal Λ β-decay (98.3%) sample the change in the value of $g_a(0)/g_v(0)$ is less than 0.001.

The remaining background comes from events in which the negative particle is an electron. An example of such a background is

$$\bar{K}_s \to \pi^0 + e^+ + e^- + \gamma \ ,$$

where the e^+ is missed by the Cherenkov counter. These events were all removed by the last cut in Table II (see Sec. IV C). Also possible is the decay

$$K_L \to \pi^+ + e^- + \bar{\nu} \ .$$

A Monte Carlo simulation for the measured Cherenkov-counter efficiency showed this process would result in a 1.9% background and decreased $g_a(0)/g_v(0)$ by 0.006 with an uncertainty of less than 0.001. Accordingly this correction is included in the final value for $g_a(0)/g_v(0)$.

F. Radiative corrections

The radiative corrections to $\Lambda \to pe^-\bar{\nu}$ as calculated by Garcia and Kielanowski[12] were included in the expression for $d^2\Gamma/dE_e^* d(\cos\theta_{ev}^*)$ [Eq. (1.3)]. These corrections are small and have a negligible effect on the value of $g_a(0)/g_v(0)$.

About 2% of a radiation length of material existed between the decay point and the electron detectors. The effect of bremsstrahlung in the material, which reduces the measured momentum of the electron without changing its direction was calculated to increase the value of $g_a(0)/g_v(0)$ by almost 2σ with an uncertainty of less than

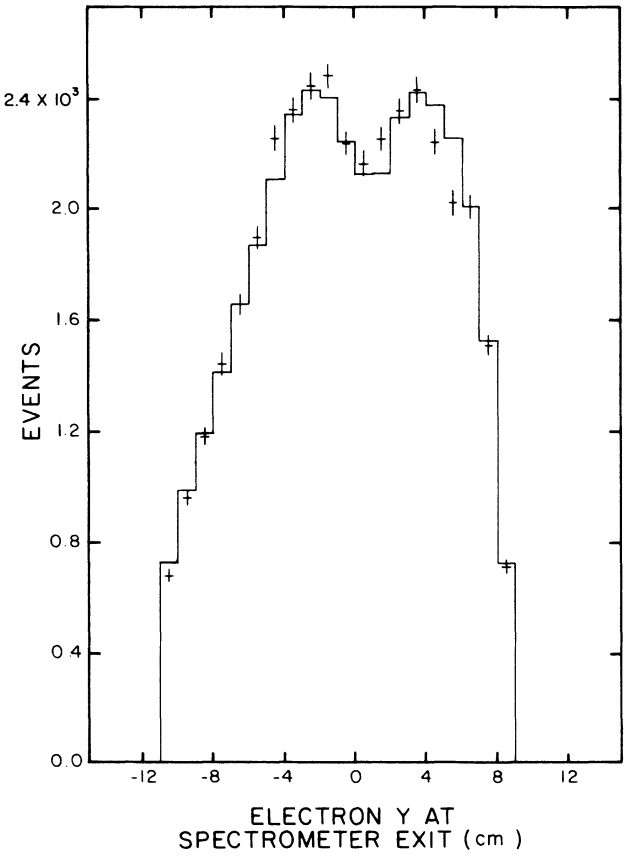

FIG. 11. The electron y distribution at the exit of the spectrometer magnet. The size of each bin is 1 cm. This figure refers to the final Λ β-decay sample. The data points are shown with error bars; the solid line is a Monte Carlo simulation.

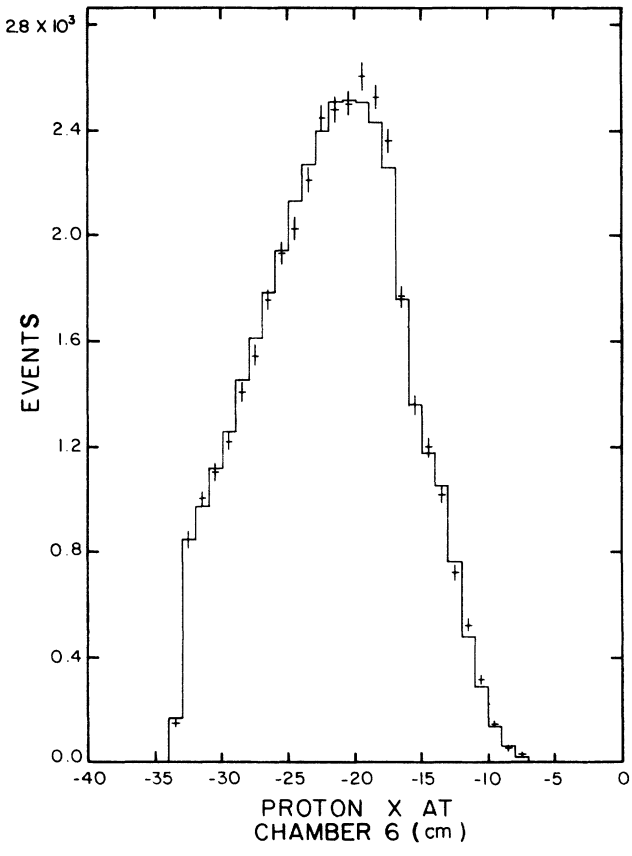

FIG. 12. The proton x distribution at chamber 6. The size of each bin is 1 cm. This figure refers to the final Λ β-decay sample. The data points are shown with error bars; the solid line is a Monte Carlo simulation.

0.002. A correction for this effect is included in the final result.

IV. DATA ANALYSIS

A. Kinematics

We consider three reference frames: the laboratory, the Λ rest frame, and the Q rest frame. We illustrate our notation by giving the momentum of the neutrino in the three frames. They are p_ν, p_ν^*, and $\tilde{p}_\nu$, respectively.

From the expression for the differential decay rate in the Λ rest frame, given in Eq. (1.3) and in Appendix A, the quantity of interest $g_a(0)/g_v(0)$ is only contained in term T. Although we use the complete expressions in our analysis one should note that the variation of T over the Dalitz plot due to the terms $(q/M_\Lambda)^2$, $(q/M_a)^2$, and $(q/M_v)^2$ is small (less than 2%). To illustrate, if one neglects the q^2 variation then

$$T=[g_v(0)]^2[T_1(1-\cos\theta_{ev}^*)+T_2(1+\cos\theta_{ev}^*)] ,$$

$$T_1=[2(E_e^*-E_\nu^*)]XY/M_\Lambda+[1/2(1+r)^2]Y^2 ,$$

$$T_2=1+Y^2 .$$

In this approximation, $r=(M_p/M_\Lambda)$ and

$$Y=g_a(0)/g_v(0), \quad w=g_w/g_v(0), \quad X=1+(1+r)w .$$

The only term which depends on the electron and neutrino energy is the XY term of T_1. Since $(q/M_a)^2,(q/M_v)^2$ are in fact small, the important variation over the Dalitz plot is contained in the XY term. After some algebra and using the Lorentz transformation between the Λ rest frame and the Q rest frame (β is the velocity of the Λ in the Q rest frame)

$$E_e^*=\gamma\tilde{E}_e(1-\beta\bar{x}) ,$$

$$p_{e\|}^*=\gamma\tilde{E}_e(\bar{x}-\beta) ,$$

where $\gamma=(M_\Lambda-E_\nu^*)/M_Q$ and $\bar{x}=\cos\tilde{\theta}_{ev}$. Rewriting Eq. (1.3) using the expressions in Appendix A (E_M^* is the maximum electron energy in the Λ rest frame) and transforming into the Q frame we find

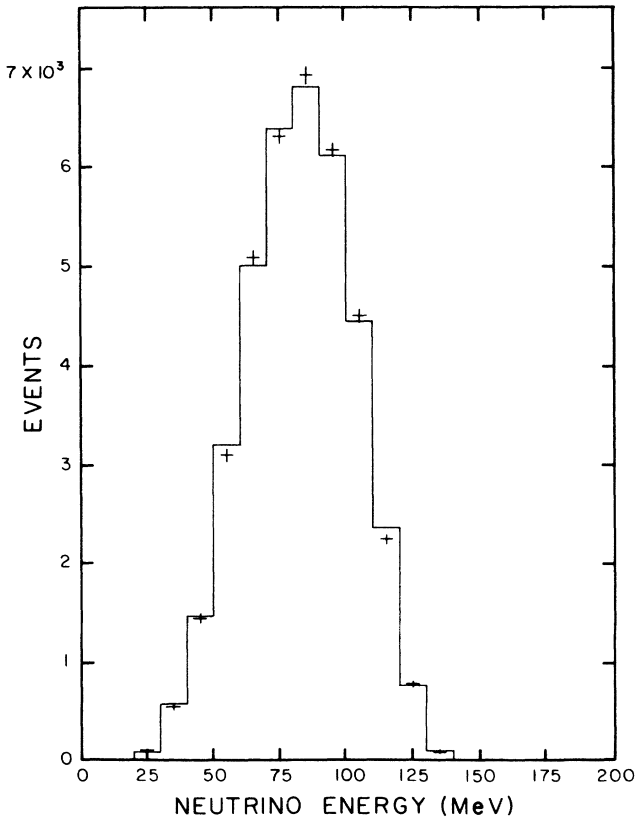

FIG. 13. The energy of the neutrino in the Λ center-of-mass system. The size of each bin is 10 MeV. This figure refers to the final Λ β-decay sample. The data points are shown with error bars; the solid line is a Monte Carlo simulation.

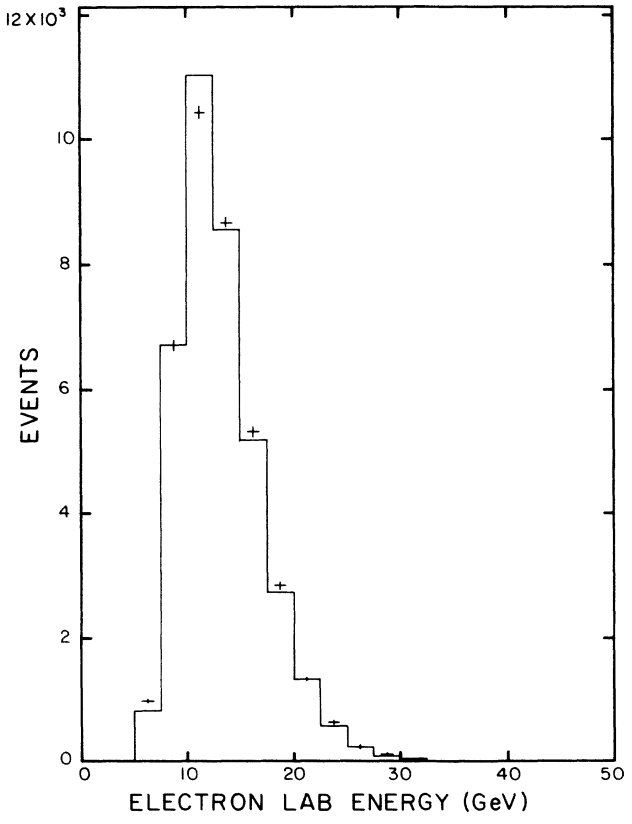

FIG. 14. The electron laboratory energy distribution. The size of each bin is 2.5 GeV. This figure refers to the final Λ β-decay sample. The data points are shown with error bars; the solid line is a Monte Carlo simulation.

$$
\begin{aligned}
d^2\Gamma/dE_\nu^* d\tilde{x} &= [(M_\Lambda E_\nu^*)^2(E_M^*-E_\nu^*)^2/(M_\Lambda-2E_\nu^*)^2] \\
&\quad\times[T_a(1-\tilde{x})+T_b(1+\tilde{x})] , \\
T_a &= [\tfrac{1}{2}(1-r)^2-\lambda]X^2+2[(E_M^*-2E_\nu^*)/M_\lambda+\lambda]XY \\
&\quad +[\tfrac{1}{2}(1+r)^2-\lambda]Y^2 , \\
T_b &= [1+2(q/M_v)^2-2\lambda w^2+Y^2](1-2E_\nu^*/M_\Lambda) , \\
\lambda &= [E_\nu^*(E_M^*-E_\nu^*)/M_\Lambda(M_\Lambda-2E_\nu^*)](1-\tilde{x}) \\
&= q^2/(2M_\Lambda^2) .
\end{aligned}
\tag{4.1}
$$

We have rewritten the expression for the differential decay rate to make explicit the terms which depend linearly on $Y=g_a(0)/g_v(0)$. Note that quantities from both the Λ rest frame and the Q frame are used here. This form makes it clear how to determine the sign of $g_a(0)/g_v(0)$: the data should be binned in terms of the energy of the neutrino in the Λ rest frame.

B. Ambiguity resolution in the Q rest frame

Measurement of each event yields a vector momentum $\mathbf{p}_e$ for the electron, $\mathbf{p}_p$ for the proton, and a decay point (x_d,y_d,z_d). The Λ direction $\hat{\lambda}$ is taken to be the line joining the decay point to a point at the center of the allowed region of the production target (x_B,y_B,z_B). Knowing the Λ direction, and the proton and electron momenta, gives a zero constraint fit for the Λ β decay.

Figure 16 shows the decay in the Q rest frame. In this frame the kinematics are described by the following equations:

$$
\begin{aligned}
&\tilde{\mathbf{p}}_\Lambda=\tilde{\mathbf{p}}_\nu, \quad |\tilde{\mathbf{p}}_\Lambda|=|\tilde{\mathbf{p}}_\nu|=(M_\Lambda^2-M_Q^2)/2M_Q , \\
&\tilde{\mathbf{p}}_e=-\tilde{\mathbf{p}}_p, \quad |\tilde{\mathbf{p}}_e|=|\tilde{\mathbf{p}}_p|=(M_Q^2-M_p^2)/2M_Q .
\end{aligned}
\tag{4.2}
$$

Equation (4.1) shows the differential decay rate as a function of $\tilde{x}=\cos\tilde{\theta}_{ev}$. To obtain $g_a(0)/g_v(0)$ we measure an asymmetry

$$
\tilde{\alpha}_{ev}=\frac{2[\Gamma(0<\tilde{x}<1)-\Gamma(-1<\tilde{x}<0)]}{\Gamma(-1<\tilde{x}<1)} .
$$

The asymmetry in the distribution of $\tilde{x}$ is as sensitive to the value of $g_a(0)/g_v(0)$ as the asymmetry in $\cos\theta_{ev}^*$. Figure 17(a) shows $\tilde{\alpha}_{ev}$ as a function of $g_a(0)/g_v(0)$ for the conditions of the present experiment [Fig. 17(b) shows the corresponding relation for α_{ev}]. All the momenta defined above can be divided into components perpendicular or parallel to the direction of p_Q. In particular,

$$
\tilde{\mathbf{p}}_e=\tilde{\mathbf{p}}_{e\perp}+\tilde{p}_{e\parallel}\hat{\mathbf{q}}, \quad \tilde{\mathbf{p}}_\nu=\tilde{\mathbf{p}}_\Lambda=\tilde{\mathbf{p}}_{\nu\perp}+\tilde{p}_{\nu\parallel}\hat{\mathbf{q}} ,
\tag{4.3}
$$

where the transverse components are Lorentz invariant and thus are directly measured in the laboratory system

$$
\begin{aligned}
\tilde{x} &= (\tilde{\mathbf{p}}_e\cdot\tilde{\mathbf{p}}_\nu)/(|\tilde{p}_e\tilde{p}_\nu|) \\
&= (\tilde{\mathbf{p}}_{e\perp}\cdot\tilde{\mathbf{p}}_{\nu\perp})/(|\tilde{p}_e\tilde{p}_\nu|) \\
&\quad +(\tilde{p}_{e\parallel}\tilde{p}_{\nu\parallel})/(|\tilde{p}_e\tilde{p}_\nu|) .
\end{aligned}
\tag{4.4}
$$

The two-solution ambiguity present in our zero-constraint fit essentially means that the sign of the term involving the parallel components in the above equation is unknown. Since we are trying to determine an asym-

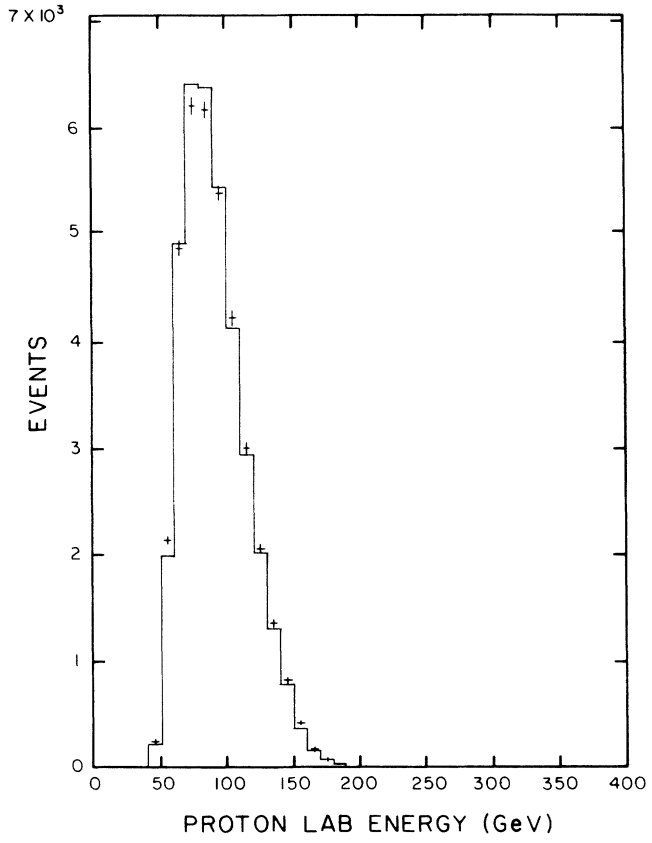

FIG. 15. The proton laboratory energy distribution. The size of each bin is 10 GeV. This figure refers to the final Λ β-decay sample. The data points are shown with error bars; the solid line is a Monte Carlo simulation.

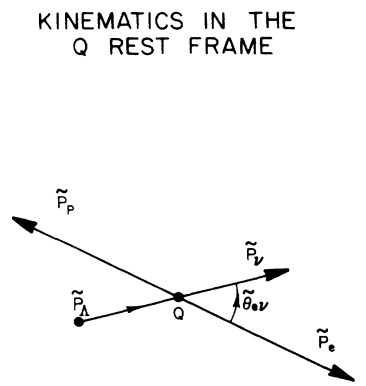

FIG. 16. The electron, proton, Λ, and neutrino momenta are given in the Q rest frame.

metry in $\tilde{x}$, this is almost as bad as knowing nothing about the parallel term. Thus all the useful information about the event is contained in the perpendicular term. Referring to Figs. 16 and 1 we see that

$$(\tilde{\mathbf{p}}_{e\perp}\cdot\tilde{\mathbf{p}}_{\nu\perp})/(|\tilde{p}_e\tilde{p}_\nu|)=|\tilde{\mathbf{p}}_{e\perp}||\tilde{p}_{\nu\perp}|\cos(\Phi)/(|\tilde{p}_e\tilde{p}_\nu|)\ . \quad (4.5)$$

Since $d^2\Gamma/dE_\nu^* d\tilde{x}$ is of the form $1+\tilde{\alpha}_{e\nu}\tilde{x}$ it should be of the form $1+a\cos(\Phi)$ where the value of a is a function of the value of $g_a(0)/g_v(0)$.

C. Uncertainties in the measurement of Φ

We next discuss in some detail how accurately Φ is known. As seen from Fig. 1, Φ is the angle between line $Q\Lambda\bar{\nu}$ and pQe. The angle between line pQe and the x axis is the azimuthal angle Φ_e of the charged-particle decay plane and is well measured except for the very forward eQ decays. These decays have small opening angles between the proton and the electron and cannot be reliably separated by the 2-mm wire spacing of the proportional chambers. Their topology is similar to $\gamma \to e^+e^-$ events which are a possible background in the Λ β-decay sample. For such events $|\mathbf{p}_{e\perp}|/\tilde{p}_e$ is small and the first term in Eq. (4.3) for $\tilde{x}$ is small compared to the second term whose sign is unknown. Thus these events, besides having relatively large uncertainties in Φ_e, contain little information about $\tilde{\alpha}_{e\nu}$. For these reasons events where $|\tilde{p}_{e\parallel}|/\tilde{p}_e > 0.95$ were cut from the data sample. Figure 18, a plot of the difference between Φ_e as generated by the Monte Carlo simulation and after it is smeared by the apparatus resolution, shows the resolution of Φ_e after this cut.

The effect of the uncertainty in the measurement of the line $Q\Lambda\bar{\nu}$ on the azimuthal angle Φ_Q of the $\Lambda \to Q\bar{\nu}$ decay is more serious. This uncertainty is best understood by taking the plane of Fig. 1 to be the plane containing the production target. Figure 19 shows $Q=(x_Q,y_Q)$ surrounded by 1σ and 2σ error ellipses and $\Lambda=(x_\Lambda,y_\Lambda)$ surrounded by a circle of radius 1.5 mm (the size of the production target). Λ has to be somewhere inside the real target while the real Q for most events will be somewhere inside of the 2σ ellipse. Figure 19 is drawn to scale for the distance between Λ and Q to be equal to the average for Λ β sample (about 7 mm). It is clear that there can be considerable uncertainty in Φ_Q. For events where the distance between Λ and Q is small and the target circle is contained inside the 2σ ellipse, Φ_Q is virtually unknown. Such events with small distance between Λ and Q corre-

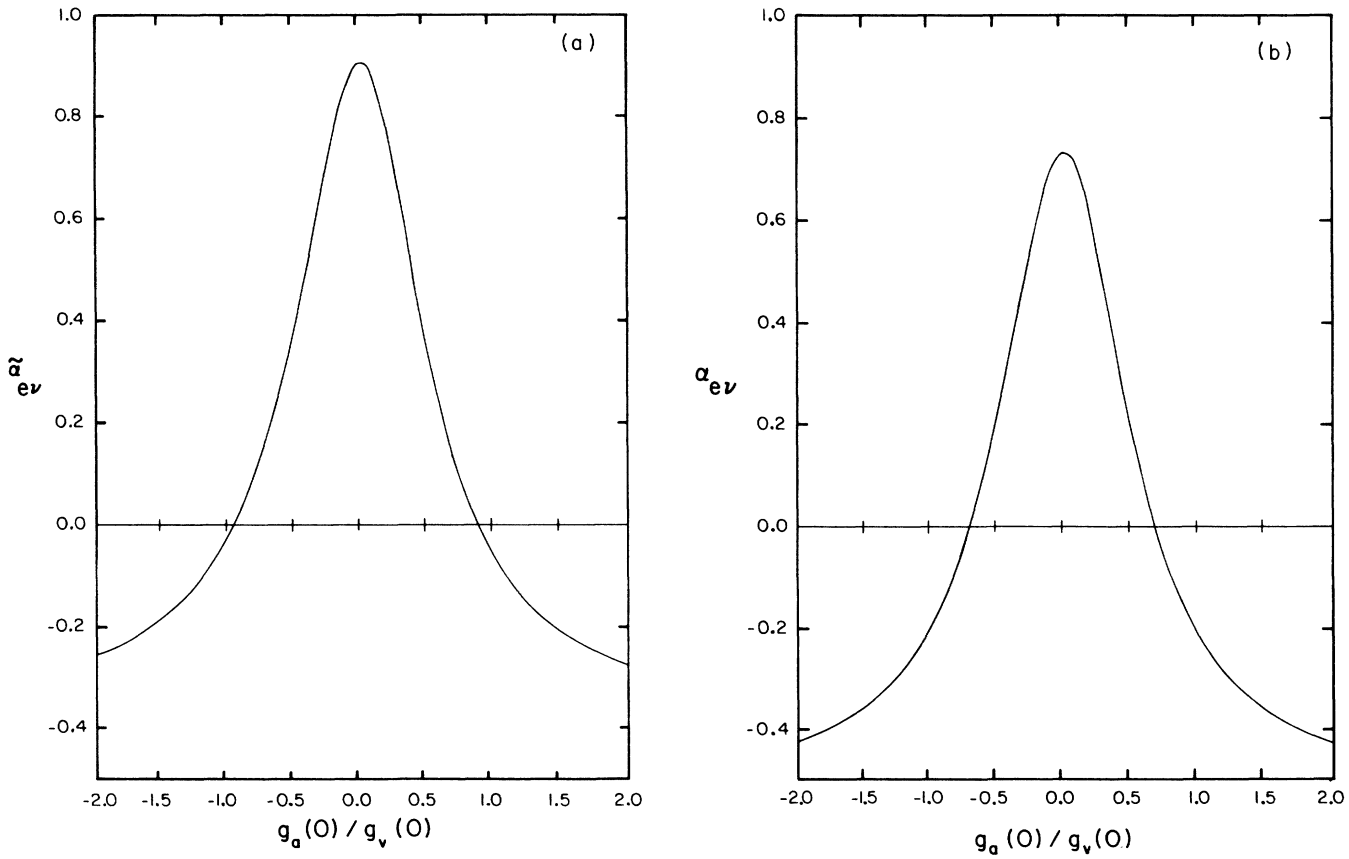

FIG. 17. (a) The asymmetry parameter $\tilde{\alpha}_{e\nu}$ is given as a function of $g_a(0)/g_v(0)$. (b) The asymmetry parameter $\alpha_{e\nu}$ is given as a function of $g_a(0)/g_v(0)$.

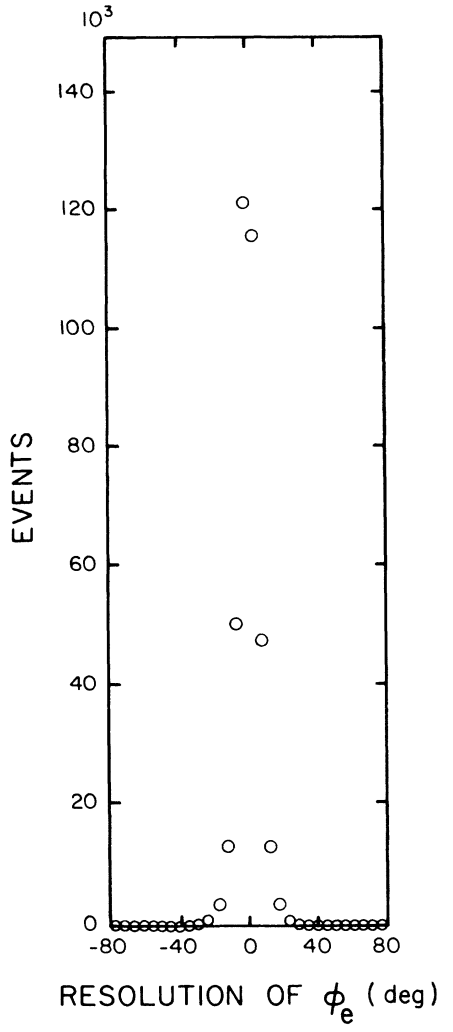

FIG. 18. This figure shows the angular resolution (difference between true angle and reconstructed angle as determined by the Monte Carlo simulation) for the angle Φ_e (see Fig. 1).

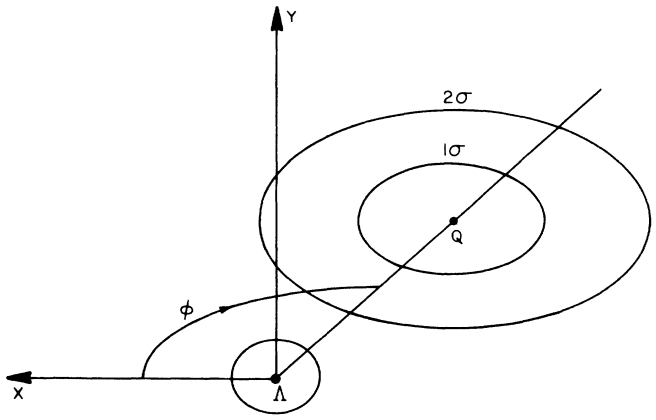

FIG. 19. The plane of Fig. 1 is taken to be the production plane. The points Λ and Q are shown. The Λ point is the center of a circle of radius equal to the radius (1.5 mm) of the production target. The Q point is surrounded by 1σ and 2σ error ellipses. The 1σ error ellipse has semiaxis of 3.5 mm and 2.0 mm in x and y, respectively.

spond to forward Q's in the Λ rest frame for $\Lambda \to Q\bar{\nu}$ decays. For these events $|\tilde{\mathbf{p}}_{\nu\perp}|/\tilde{p}_\nu$ is small and the first term in Eq. (4.4) is small compared to the second. Thus these events would contribute little to the measurement of $\tilde{\alpha}_{e\nu}$ even if it were possible to measure Φ_Q accurately. Also they are kinematically similar to the $\Lambda \to p\pi^-$ decays which are the main background in the Λ β sample. For the above reasons, events in which the Λ origin lay within the 2σ ellipse about Q were cut. While this is a serious cut removing about 35% of the Monte Carlo β decays, it is very useful in eliminating background and has little effect on the uncertainty in $\tilde{\alpha}_{e\nu}$. Figure 20 shows the resolution of Φ_Q after this cut.

Next we discuss systematic errors in Φ. Since fixed Φ does not correspond to any fixed direction in space, the results of this experiment should be relatively insensitive to any fixed spatial bias (e.g., left-right or up-down) of the

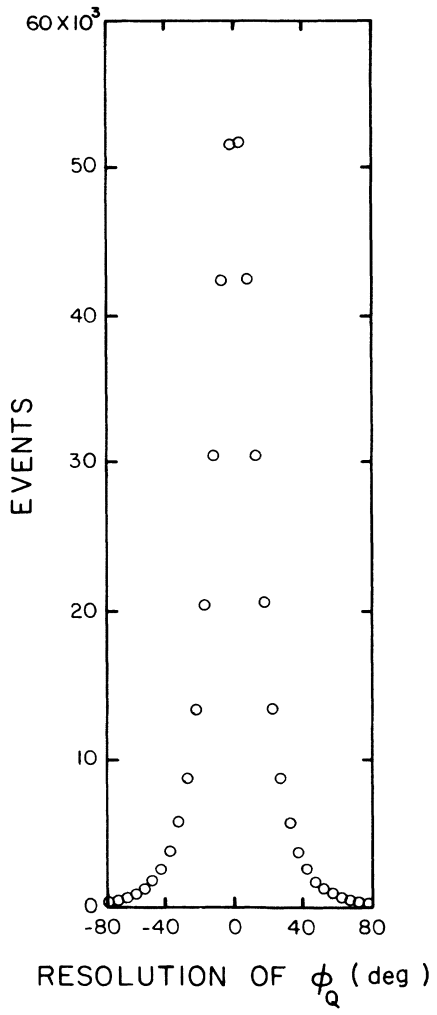

FIG. 20. This figure shows the angular resolution (difference between true angle and reconstructed angle as determined by the Monte Carlo simulation) for the angle Φ_Q (see Fig. 1).

equipment. The distribution of Φ can be distorted, however, by small systematic errors in p_e, p_p or the decay vertex. These could be caused by small misalignments of the spectrometer chambers or by nonuniform components of the magnetic field of the spectrometer magnet. An accurate measurement of Φ_Q depends on a bias-free measurement of $x_Q - x_\Lambda$ and $y_Q - y_\Lambda$, as can be seen from Fig. 18. These distances average about 5 mm and to calculate them the measured tracks have to be extrapolated 18 m from the nearest chambers, so that a very small error could cause a significant shift in Φ.

Fortunately there is a way of accurately measuring such a distortion if it exists. Together with the Λ β-decay sample we have a large $\Lambda \to p\pi^-$ sample. For these events the Q corresponds to the Λ and (x_Q, y_Q) should be the same as (x_Λ, y_Λ), the center of the production target within measuring errors. A subsample of 750 000 of the $p\pi^-$ decays were divided into 80 bins, 5 in p_π and 16 in Φ_π (corresponding to Φ_e in β decay). We compare the projected position at the production target for the $p\pi^-$ data with the $p\pi^-$ Monte Carlo simulation (this Monte Carlo simulation is similar to the one for β decays and is not discussed further). These distributions were found to differ from each other by as much as 2 mm at low p_π which is more than their statistical uncertainties. The data in each of the 80 bins were corrected such that the target pointing agreed with the Monte Carlo average for that bin. The Λ β-decay events were then identically binned and the corresponding bins were modified by the same amounts. This target pointing correction changed the overall value of $g_a(0)/g_v(0)$ by 0.03. The uncertainty of this correction introduces a possible systematic error which we estimate to be less than 0.006.

D. Summary of data selection

Table II gives the effect of important cuts on the data compared to the Monte Carlo simulation. We begin with 98 736 events that were selected to satisfy the basic Λ β-decay topology as described in Sec. III A. The number of Monte Carlo events were chosen to give a final Monte Carlo sample 10 times larger than the final data sample. The first three cuts in the table are additional topology cuts described in Sec. III A. Cut 4 requires that the reconstructed Λ momentum vector pass through the 4-mm diameter collimator. The kinematic circle cut essentially requires that the Λ decay conserve transverse momentum. Both cuts 4 and 5 are described in Sec. III C. The cut which eliminates most of the remaining data, cut 6 (discussed in detail in Sec. IV C), essentially requires that the neutrino opening angle not be too small. This cut eliminates events in which Φ is not well determined and also $\Lambda \to p\pi^-$ background. Cut 7 reduces $p\pi^-$ background events by requiring a minimum decay opening angle if the mass of the vee is within 3σ of the Λ mass to ensure that the event is very well measured. The next four cuts, 8, 9, 10, and 11 are slightly tighter fiducial cuts within the limiting apertures of the spectrometer to protect against small differences between data and Monte Carlo distributions. Finally, cut 12 requires that the electron opening angle be large enough to accurately determine Φ and reject photon conversions as described in Sec. IV C. The data selection combined with the acceptance of the spectrometer yields a sensitivity to Λ β decay which is relatively uniform over the allowed kinematics. The efficiency of the experiment for measuring Λ β decays which occur in the decay volume is given in Table III as a function of $\cos\theta^*_{ev}$ and $E_\nu/E_{\nu\,\max}$. As can be seen, the experiment spans most of the allowed kinematic space.

E. Summary of systematic errors

Specific sources of systematic errors were investigated and found to be negligible compared to our statistical error for $g_a(0)/g_v(0)$. Residual background described in Sec. III E could contribute as much as 0.001 to the error. Uncertainty in the radiative corrections described in Sec. III F could introduce an error as large as 0.002. Uncertainties in momentum reconstruction described in Sec. IV C could lead to an error in Φ giving a systematic error in the result of less than 0.006. Error introduced by q^2 dependence of the form factors are more difficult to estimate since the form factors are not known from first principles. We include terms of order q^2/M^2 as described in Sec. I A. Since our largest $q^2 = 0.03$ $(\mathrm{GeV}/c)^2$, the error introduced by neglecting the next term in the expansion usually used is less than 0.001. Since systemat-

TABLE III. Detection efficiency. E_ν is neutrino energy, and $E_{\nu\,\max}$ is maximum neutrino energy.

$\cos(\theta^*_{ev})$	$E_\nu/E_{\nu\,\max}$ 0.0	0.1	0.2	0.3	0.4	0.5	0.6	0.7	0.8	0.9
−1.	0.00	0.01	0.04	0.09	0.13	0.14	0.12	0.06	0.01	0.00
−0.8	0.00	0.01	0.04	0.09	0.13	0.15	0.12	0.06	0.01	0.00
−0.6	0.00	0.01	0.04	0.09	0.14	0.15	0.12	0.05	0.01	0.00
−0.4	0.00	0.01	0.04	0.10	0.14	0.15	0.12	0.05	0.00	0.00
−0.2	0.00	0.01	0.04	0.10	0.14	0.15	0.11	0.05	0.00	0.00
0.0	0.00	0.01	0.04	0.10	0.14	0.15	0.11	0.05	0.00	0.00
0.2	0.00	0.01	0.04	0.10	0.14	0.14	0.11	0.04	0.00	0.00
0.4	0.00	0.01	0.04	0.09	0.13	0.14	0.10	0.04	0.00	0.00
0.6	0.00	0.01	0.04	0.09	0.13	0.13	0.09	0.03	0.00	0.00
0.8	0.00	0.01	0.04	0.09	0.13	0.13	0.09	0.03	0.00	0.00

ic errors estimates are not statistical, there is no *a priori* method of combining them. If we estimate a systematic error in $g_a(0)/g_v(0)$ by adding them in quadrature, we arrive at a possible systematic error of 0.006 from known sources.

V. RESULTS

A. Standard analysis

The result of the standard analysis for $\Lambda \rightarrow p e^- \bar{\nu}$ in which both solutions for each event are plotted as a function of $\cos(\theta^*_{ev})$ is given in Fig. 21. The two solutions are weighted according to the Λ momentum spectra and compared to the Monte Carlo simulation. The result is $g_a(0)/g_v(0)=0.720\pm0.018$ with a $\chi^2=10.1$ for 19 bins. The expected χ^2 is 9.5 since both solutions are used, which effectively gives 9.5 degrees of freedom (DF). In the standard analysis we have used the conserved-vector-current (CVC) value of $w=0.97$.

B. New analysis

In Sec. I B we argued that the $\cos(\Phi)$ distribution is more sensitive to $g_a(0)/g_v(0)$ than $\cos(\theta^*_{ev})$. The comparison of data and Monte Carlo simulation for $\cos(\Phi)$ is given in Fig. 22 as a function of $g_a(0)/g_v(0)$. The minimum in χ^2 is 19.6 for 19 DF corresponding to $g_a(0)/g_v(0)=0.719\pm0.016$ and an electron-neutrino correlation of $\alpha_{ev}=-0.017\pm0.013$. The above results were obtained with $w=0.97$ the value given by the CVC hypothesis. The final $\cos\Phi$ distribution for $g_a(0)/g_v(0)$ is shown in Fig. 23 for the minimum value of χ^2.

C. A global test for systematic errors

To test systematics introduced by our analysis, $d^2\Gamma/dE^*_\nu d\tilde{x}$ from the data and Monte Carlo simulation were fit to the simple function $1+a\cos(\Phi)+b\sin(\Phi)$. Here the $\sin(\Phi)$ term is orthogonal to the expected behavior of the data due to β-decay physics, $\cos(\Phi)$. The $\sin(\Phi)$ term must be introduced by distortions of the data due to apparatus acceptances or analysis procedure. It is not necessary that this expression fit perfectly since data distortions could require higher-order terms in $\sin(\Phi)$ and $\cos(\Phi)$. Nevertheless, the simple function should fit the data and the Monte Carlo simulation equally well if no large systematic errors due to unknown sources are present in the data. We used this technique to test for a

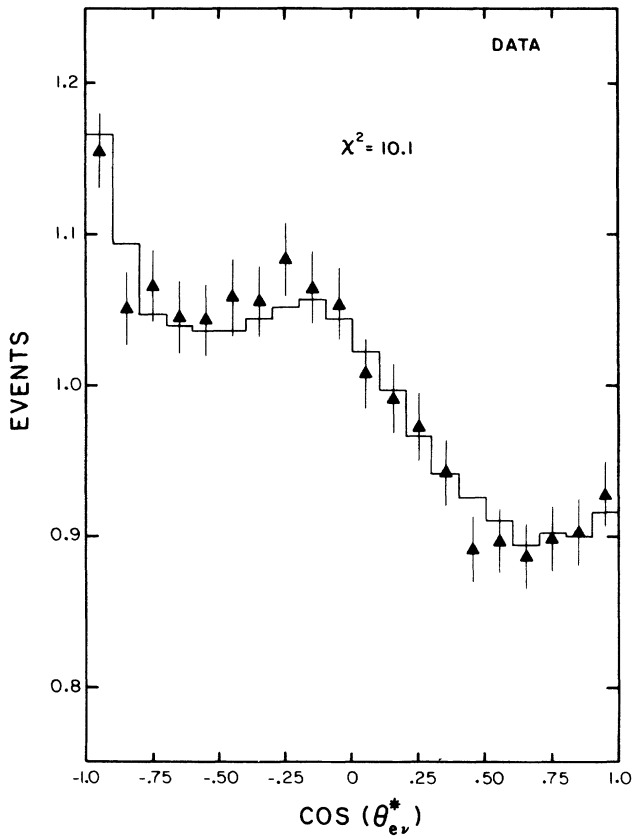

FIG. 21. The ev correlation for $\Lambda \rightarrow p e^- \bar{\nu}$. The data points are shown with error bars; the solid line is the Monte Carlo simulation. The vertical scale is normalized as in Fig. 2. The size of each bin is 0.1. The fit has a $\chi^2=10.1$ for 9.5 DF.

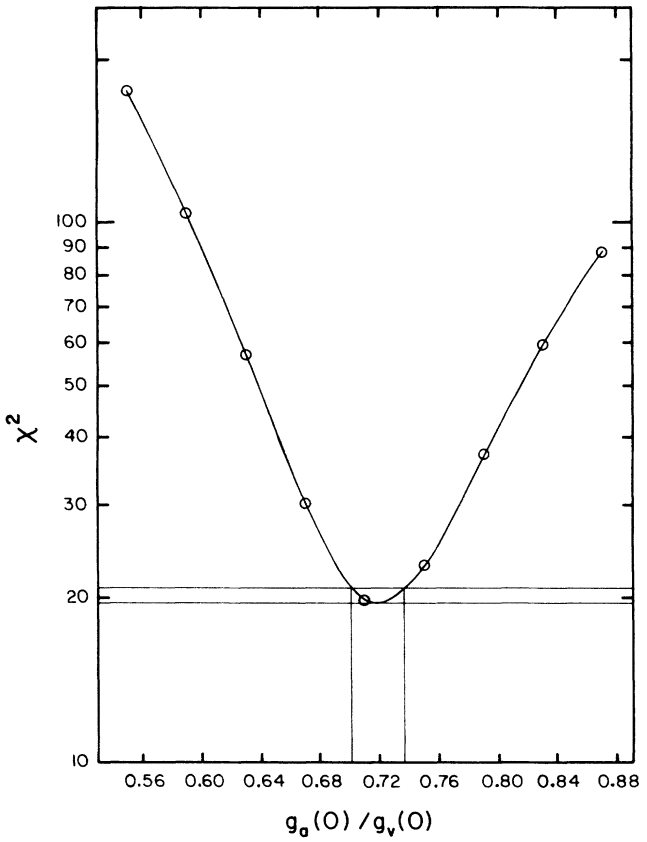

FIG. 22. The χ^2 for the comparison of the data and the Monte Carlo solutions is plotted as a function of $g_a(0)/g_v(0)$. The horizontal lines represent χ^2 changing by ±1. The vertical lines represent $\pm1\sigma$.

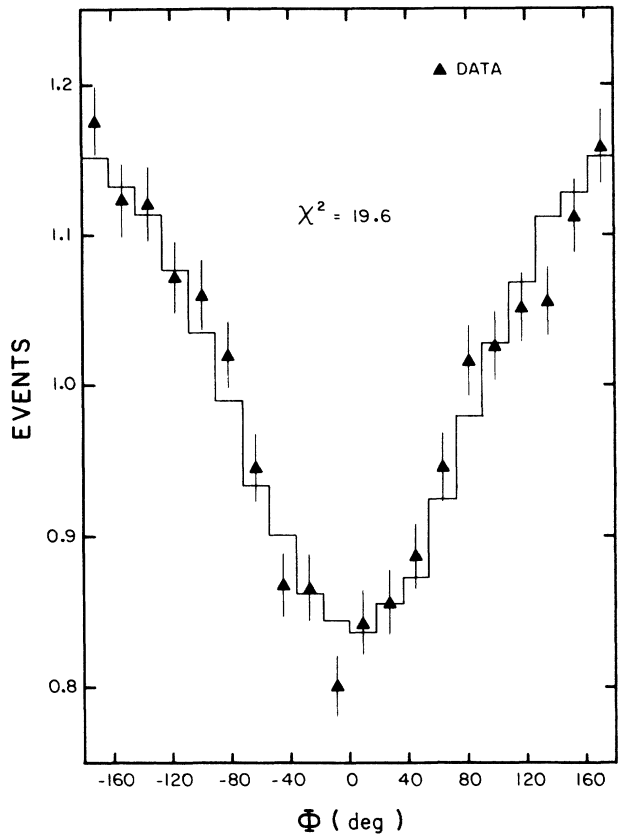

FIG. 23. The cosΦ distribution at χ^2 minimum. The data points are shown with error bars, and the solid line is the Monte Carlo simulation. The vertical scale is normalized as in Fig. 2. The size of each bin is 18 degrees. The fit has a $\chi^2=19.6$ for 19 DF.

known possible problem, a constant error in the location of the point Q

$$x'_Q = x_Q + \delta_x, \quad y'_Q = y_Q + \delta_y \ .$$

The effect of such a constant error on an otherwise symmetric Gaussian distribution is given in Appendix B. In order to see if such an error existed, the β-decay sample was divided into eight bins in Φ_e and the distribution $N_j(\Phi)$ for each of these bins was assumed to be of the form

$$N_j(\Phi) = 1 + a_j \cos(\Phi) + b_j \sin(\Phi) \ .$$

The same was done to a sample of Monte Carlo β decays and δ_x and δ_y were picked to minimize the difference, in the sense of least squares, between the fitted parameters for the real data and the Monte Carlo samples. We obtained the displacements $\delta_x = 0.13 \pm 0.04$ mm and $\delta_y = 0.07 \pm 0.04$ mm which were used in the final analysis of the data.

To test for the existence of unknown systematic errors, Monte Carlo events with $g_a(0)/g_v(0)$ and α_{ev} equal to the result obtained from the data were fit to the distribution $1 + a\cos(\Phi) + b\sin(\Phi)$. We obtained $a = -0.1591 \pm 0.0023$ and $b = -0.0062 \pm 0.0023$ with $\chi^2 = 25.1$ for 18 DF as is shown in Fig. 24(a). The same fit was performed for the data yielding $a = -0.1567 \pm 0.0072$ and $b = -0.0082 \pm 0.0073$ with $\chi^2 = 23.1$ for 18 DF and is shown in Fig. 24(b). Since the Monte Carlo events and the data fit the simple function equally well, $\chi^2/N_{\rm DF} = 1.3$ vs 1.4, and give the same coefficients for $\sin(\Phi)$ and $\cos(\Phi)$ terms, there is no evidence of an unknown systematic error from this test. In addition, the coefficient of the $\sin(\Phi)$ term is very small showing that the result, which varies as $\cos(\Phi)$, is relatively insensitive to apparatus acceptance.

D. Consistency of results

Although the fits to the β-decay hypothesis are excellent using either $\cos\theta^*_{ev}$ distributions [$g_a(0)/g_v(0) = 0.720 \pm 0.018$, $\chi^2/N_{\rm DF} = 1.06$] or $\cos(\Phi)$ distributions [$g_a(0)/g_v(0) = 0.719 \pm 0.016$, $\chi^2/N_{\rm DF} = 1.03$] and a global test for systematic errors gives no indication of unknown systematic errors; such errors would not be detected if they conspire to maintain the shape of the underlying physical process. To test that possibility we have examined our results as a function of many other variables. The results as a function of neutrino center-of-mass energy are only marginally consistent with a $\chi^2 = 11.6$ for an expected $\chi^2 = 2$. This discrepancy can be removed by letting g_w deviate from the CVC value (see Sec. V F). Figures 25(a)–25(d) correspond to $g_a(0)/g_v(0)$ as a function of neutrino energy in the Λ rest frame, as a function of z vertex, as a function of the momentum of the Q particle, and as a function of $M_{p\pi}$, respectively. Figure 25(e) shows the best quality events (based on the lead-glass in-

TABLE IV. Experimental results.

	N	$\lvert g_a/g_v \rvert$
This experiment	37286	0.731 ± 0.016 ($w = 0.15$)
		0.719 ± 0.016 ($w = 0.97$)
Bourquin *et al.*	7111	0.70 ± 0.03
Wise *et al.*	10000	0.734 ± 0.031
Lindquist *et al.*	441	0.53 ± 0.09
Burnett *et al.*	405	0.47 ± 0.09
Althoff *et al.*	817	0.63 ± 0.06
Baggett *et al.*	352	0.74 ± 0.09
Canter *et al.*	141	0.75 ± 0.15
Maloney *et al.*	148	0.72 ± 0.14

formation and also on the xenon-chamber information) and the other events. Finally, Fig. 25(f) shows $g_a(0)/g_v(0)$ for the topologies of electron and proton crossing or not crossing.

E. Sign of g_a/g_v

As indicated in Sec. IV A the sign of $g_a(0)/g_v(0)$ can be determined by binning the data in E_ν. The results are illustrated in Fig. 26(a) which is for $g_a(0)/g_v(0)$ positive [Fig. 26(a) is the same as Fig. 25(a)] while Fig. 26(b) is for $g_a(0)/g_v(0)$ negative. The total χ^2 is 11.6 for $g_a(0)/g_v(0)$ positive and 49.4 for $g_a(0)/g_v(0)$ negative where the expected χ^2 is 2. When w is taken to be 0.15 (see Sec. V F) instead of 0.97 the χ^2 for this fit is reduced to 0.9 for $g_a(0)/g_v(0)$ positive and 21 for the negative value. For either solution of w, the positive solution is favored by over 3σ.

F. Determination of g_w/g_v

The value of $w=g_w(0)/g_v(0)$ can also be determined from our data. First, we obtain the best value of $g_a(0)/g_v(0)$ for a series of values of w. This is illustrated in Fig. 27. Using these values of $g_a(0)/g_v(0)$, the data are binned in E_ν: the results are shown in Figs. 27(a)–27(e) for the values of $w=1$, 0.75, 0.50, 0.25, 0.0. A parabolic fit to the values of χ^2 as a function of w yields a minimum at $w=0.15$. This corresponds to $\chi^2=0.9$ for two degrees of freedom. The result of our analysis is $w=0.15\pm0.30$ and $g_a(0)/g_v(0)=0.731\pm0.016$. The corresponding value of the electron-neutrino correlation is $\alpha_{ev}=-0.027\pm0.013$. The consistency of the data for the value of $w=0.15$ is now very good. This is shown in Figs. 28(a)–28(f) where the same quantities are plotted as in Fig. 25.

G. Comparison with previous results

Table IV gives all published values of $g_a(0)/g_v(0)$ since 1969. There are only two other high-statistics experiments, those of Wise *et al.*[7] and Bourquin *et al.*[8] The average of all the previous experiments is $g_a(0)/g_v(0)=0.694\pm0.025$ (Ref. 15) in good agreement with our result of $g_a(0)/g_v(0)=0.719\pm0.016$ when we also assume $w=0.97$. Our result for $w=0.15\pm0.30$ is 2.7σ from the expected value of 0.97. The corresponding result from Bourquin *et al.* is $w=1.32\pm0.81$. Theoretical values of

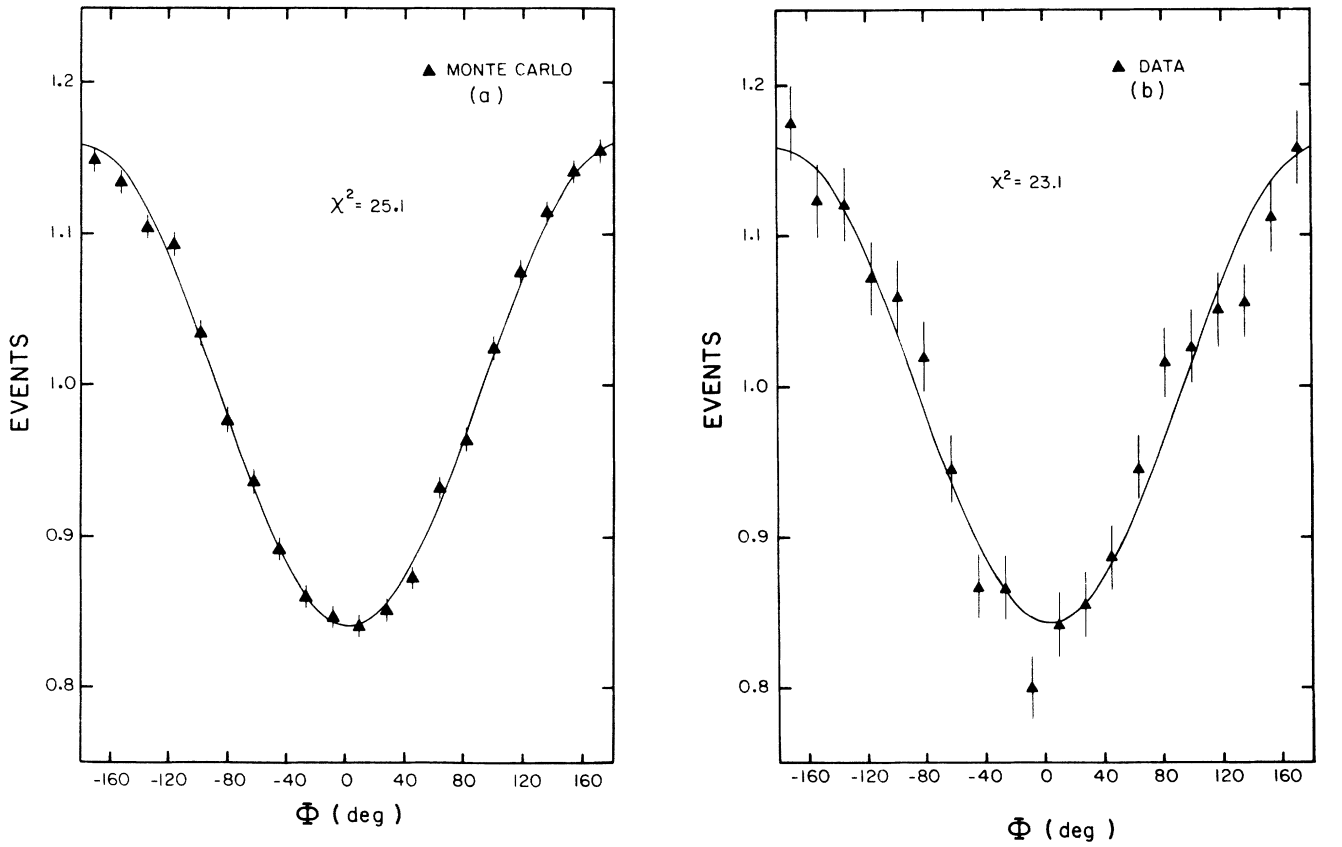

FIG. 24. (a) The Φ distribution for $\Lambda\to pe^-\bar{\nu}$. The best fit to the Monte Carlo simulation for the function $1+a\cos(\Phi)+b\sin(\Phi)$. The size of each bin is 18 degrees. The fit has a $\chi^2=25.1$ for 18 DF. (b) The best fit to the data of the same function. The fit has a $\chi^2=23.1$ for 18 DF.

the magnetic transition form factor different from the CVC hypothesis (0.973) have been predicted. Carson, Oakes, and Willcox have predicted baryon semileptonic decays using one-gluon QCD corrections to the transition amplitudes. Their prediction for $g_w(0)/g_v(0)$ is 1.32 (Ref. 16). Sirlin has related the weak and the electromagnetic form factors of the baryon octet which leads to a prediction of $g_w(0)/g_v(0)=0.76$ (Ref. 17). Lie-Svendsen and Høgaasen have used a bag-model calculation to predict $g_w(0)/g_v(0)=0.40$ (Ref. 18). This value is favored by our experiment, but clearly an even higher-statistics experiment is needed to resolve this question.

Siebert[19] has pointed out the $F+D$ determined from hyperon decays is 1.18 ± 0.02, while that determined from the asymmetry measurements of the neutron decay is

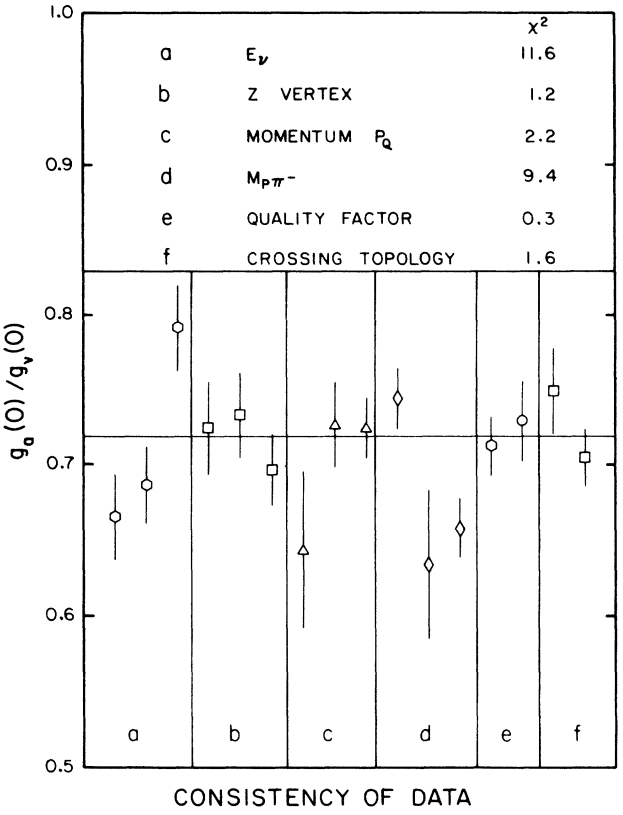

FIG. 25. The consistency of $g_a(0)/g_v(0)$ for various subsamples is displayed. For (a)–(d) there are 2 DF while (e) and (f) have 1 DF. (a) The neutrino energy: The bins are $E_\nu < 0.0725$ GeV, 0.0725 GeV $< E_\nu < 0.0916$ GeV, and $E_\nu > 0.0916$ GeV. (b) The z vertex: The bins are 200 cm $< z <$ 500 cm, 500 cm $< z <$ 800 cm, and 800 cm $<$ 1260 cm. (c) The momentum of the Q particle: The bins are $P_Q < 75$ GeV/c, 75 GeV/c $< P_Q <$ 100 GeV/c, and $P_Q > 100$ GeV/c. (d) $M_{p\pi} < M_{\Lambda-3\sigma}$, $M_{\Lambda-3\sigma} < M_{p\pi} < M_{\Lambda+3\sigma}$, and $M_{p\pi} > M_{\Lambda+3\sigma}$. (e) Quality factor: The bins are high-quality events, and other events. This information is based on the lead-glass and xenon-chamber information. (f) Topology: The bins are electron and proton trajectories noncrossing after $M3$ and crossing after $M3$.

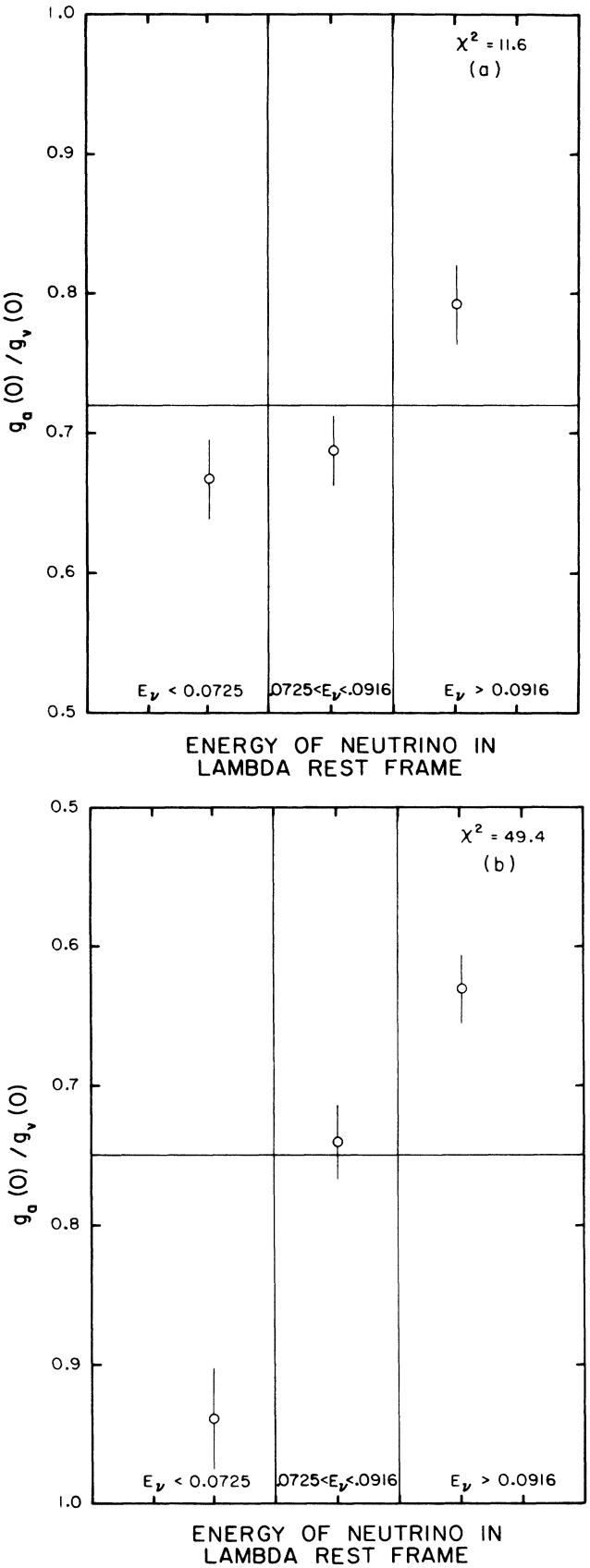

FIG. 26. Determination of the sign of $g_a(0)/g_v(0)$. The data are binned by neutrino energy. For both plots there are 2 DF: (a) $g_a(0)/g_v(0)$ positive and (b) $g_a(0)/g_v(0)$ negative.

1.263 ± 0.006, a 4σ discrepancy. The neutron decay result has been confirmed by two recent experiments. An asymmetry measurement by Klemt *et al.*[20] yields 1.265 ± 0.005, while a measurement of the lifetime by Last *et al.*[21] yields 1.277 ± 0.018. It is interesting to observe that if the previous world average electron-neutrino correlation ($F+D/3=0.694\pm0.025$) is combined with the recently improved world average for the Σ^- β-decay correlation ($F-D=-0.334\pm0.017$) (Ref. 22) the result is $F+D=1.208\pm0.038$ which is in much better agreement with the neutron result. If only the most recent high-statistics experiments are used [our result, $g_a(0)/g_v(0)=0.731\pm0.016$, and the Σ^- β-decay result of Hsueh *et al.*, $g_a(0)/g_v(0)=-0.328\pm0.019$] the value of $F+D=1.261\pm0.026$ is in excellent agreement with neutron decay.

VI. CONCLUSION

We have analyzed 37 286 Λ β decays to measure $g_a(0)/g_v(0)=+0.731\pm0.016$ ($\alpha_{e\nu}=-0.27\pm0.013$) and $w=g_w/g_v=0.15\pm0.30$. If one uses the standard value of $w=0.97$, our analysis yields $g_a(0)/g_v(0)=+0.719\pm0.016\pm0.012$ ($\alpha_{e\nu}=-0.017\pm0.013\pm0.010$). All known sources of systematic errors have been estimated to be significantly less than the statistical errors quoted. If the standard value of $w=0.97$ is indeed correct, the difference between our two results (0.731 and 0.719) would represent a measure of a systematic error of unknown origin of 0.012 in $g_a(0)/g_v(0)$ (0.010 in $\alpha_{e\nu}$). We prefer the hypothesis that the magnetic transition form factor is less than the CVC prediction.

ACKNOWLEDGMENTS

We gratefully acknowledge the help of the staff of Fermilab, in particular the Meson Laboratory, during this experiment. This work was supported in part by the National Science Foundation and the U.S. Department of Energy.

APPENDIX A

The differential decay rate in the Λ rest frame is[12]

$$d^2\Gamma/dE_e^* dx = W(E_e^*,x)T(E_e^*,x,y,w)$$

where the kinematic term is (we have set $E_e^*=p_e^*$)

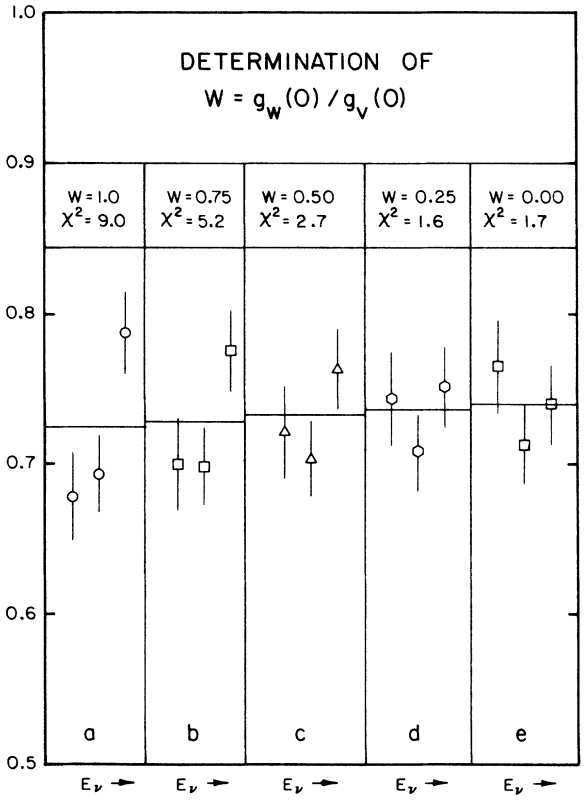

FIG. 27. Plots of $g_a(0)/g_v(0)$ as a function of neutrino energy for various values of $w=g_w(0)/g_v(0)$. The bins are $E_\nu<0.0725$ GeV, 0.0725 GeV $<E_\nu<0.0916$ GeV, and $E_\nu>0.0916$ GeV. For all plots there are 2 DF: (a) $w=1.00$, $g_a(0)/g_v(0)=0.719$, (b) $w=0.75$, $g_a(0)/g_v(0)=0.723$, (c) $w=0.50$, $g_a(0)/g_v(0)=0.726$, (d) $w=0.25$, $g_a(0)/g_v(0)=0.730$, (e) $w=0.00$, $g_a(0)/g_v(0)=0.733$.

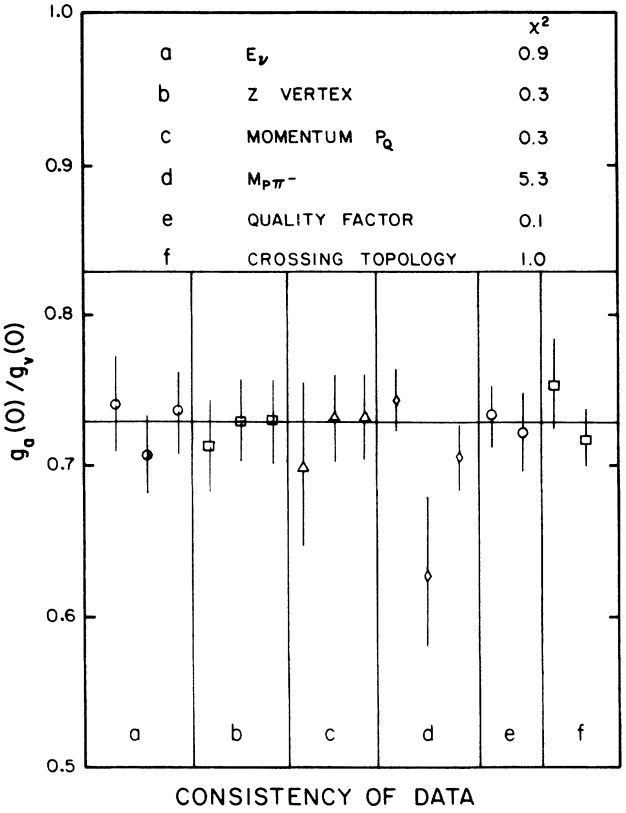

FIG. 28. The consistency of $g_a(0)/g_v(0)$ for various subsamples when $g_w(0)/g_v(0)=0.15$ is displayed The bins are the same as for Fig. 25. For (a)–(d) there are 2 DF while (e) and (f) have 1 DF.

$$W(E_e^*,x)=(E_e^*)^2(E_M^*-E_e^*)^2/[1-(1-x)(E_e^*/m_\Lambda)]^3$$

and $E_M^*=(M_\Lambda^2-M_p^2)/2M_\Lambda$ is the maximum possible electron energy, $x=\cos\theta_{ev}^*$, $y=g_a(0)/g_v(0)$ and $w=g_w/g_v(0)$. The q^2 dependence of the form factors has been given in the Introduction:

$$T/[g_v(0)]^2=T_1(1-x)+T_2(1+x) .$$

If we set

$$r=M_p/M_\Lambda ,$$

$$X=1+2(q/M_v)^2+(1+r)w ,$$

$$Y=(1+2(q/M_A)^2)y$$

then

$$T_1=\{[\tfrac{1}{2}(1-r)^2-\tfrac{1}{2}(q/M_\Lambda)^2]X^2 +2(E_e^*-E_\nu^*)XY/M_\Lambda +[\tfrac{1}{2}(1+r)^2-\tfrac{1}{2}(q/M_\Lambda)^2]Y^2\} ,$$

$$T_2=1+2(q/M_v)^2+Y^2-(q/M_\Lambda)^2w^2 .$$

APPENDIX B

The effect of a constant error in the location of a point Q on a Gaussian distribution

$$D(x_Q,y_Q)=\exp[-(x_Q^2+y_Q^2)/2\sigma^2]$$

would be to shift the distribution to the no longer azimuthally symmetric form

$$D(x_Q',y_Q')=\exp\{-[(x_Q-\delta_x)^2+(y_Q-\delta_y)^2]/2\sigma^2\} .$$

Introducing polar coordinates

$$x_Q'=r\cos(\Phi_Q), \quad y_Q'=r\sin(\Phi_Q)$$

the distribution takes the form

$$D(r,\Phi_Q)\approx\exp(-r^2/2\sigma^2)[1+(r/\sigma^2)\delta_x\cos(\Phi_Q) +\delta_y\sin(\Phi_Q)]$$

for small $\delta x,\delta y$. When the distribution is integrated over r, and Φ_Q is expressed in terms of Φ and Φ_e, one finds a distribution of the form

$$N(\Phi)\to N(\Phi)+f[-\delta_\parallel\cos(\Phi)+\delta_\perp\sin(\Phi)] ,$$

where

$$\delta_\parallel=\delta_x\cos(\Phi_e)+\delta_y\sin(\Phi_e) ,$$

$$\delta_\perp=-\delta_x\sin(\Phi_e)+\delta_y\cos(\Phi_e) ,$$

and $f=(\bar{r}/\sigma^2)=2.2\ \text{cm}^{-1}$ for our Λ β-decay sample.

---

[a]Present address: Fonar Corp., 110 Marcus Drive, Melville, NY 11747.
[b]Present address: Physics Dept., Rockefeller Univ., New York, NY 10021.
[c]Present address: Physics Dept., Univ. of Virginia, Charlottesville, VA 22901.
[d]Present address: Salomon Brothers, Inc., 41st Floor, 1 New York Plaza, New York, NY 10004.
[e]Present address: Fermilab, P.O. Box 500, Batavia, IL 60510.
[f]Present address: Los Alamos National Laboratory, Los Alamos, NM 87545.
[g]Present address: Honeywell Corp., 10400 Yellow Circle Dr., Minnetonka, MN 55343.
[h]Present address: Physics Dept., Univ. of California at Berkeley, Berkeley, CA 94720.

[1]J. Lindquist *et al.*, Phys. Rev. Lett. **27**, 612 (1971); J. Lindquist *et al.*, Phys. Rev. D **16**, 2104 (1977).
[2]T. H. Burnett *et al.*, Nuovo Cimento **34A**, 14 (1976).
[3]K. Althoff *et al.*, Phys. Lett. **37B**, 531 (1977); K. Althoff *et al.*, *ibid.* **43B**, 237 (1973).
[4]N. Baggett *et al.*, Z. Phys. **249**, 279 (1972).
[5]J. Canter *et al.*, Phys. Rev. Lett. **26**, 868 (1971).
[6]J. E. Maloney *et al.*, Phys. Rev. Lett. **23**, 425 (1969).
[7]J. Wise *et al.*, Phys. Lett. **98B**, 123 (1981).
[8]M. Bourquin *et al.* (II): Z. Phys. C **21**, 1 (1983).
[9]A. Bohm and M. Kmieck, Phys. Rev. D **31**, 3005 (1985). In the Cabibbo theory all semileptonic decays of baryons can be described using three parameters F, D, and $\sin\theta_C$. The results of their fit are $F=0.450\pm0.006$, $D=0.799\pm0.007$, and $\sin\theta_C=0.225$. For Λ decay they used an input value of $g_a(0)/g_v(0)=0.719\pm0.023$. They obtained a $\chi^2=40$ for 20 degrees of freedom; however a contribution of 16 to χ^2 comes from one measurement: $R(\Sigma^-\to\Lambda e^-\bar{\nu})$.
[10]A. Garcia, Phys. Rev. D **3**, 2638 (1971). The more standard way of writing the hadronic current has an i in front of the g_w and g_2 terms (see Refs. 7 and 8). Our sign convention is identical with Refs. 7 and 8 because an opposite convention is used by Garcia for the lepton current $[\gamma_\mu(1+\gamma_5)]$. We use the sign convention that $g_a(0)/g_v(0)=F+D$ is positive for neutron decay.
[11]M. Bourquin *et al.* (I): Z. Phys. C **12**, 307 (1982).
[12]A. Garcia and P. Kielanowski, Phys. Lett. **120B**, 214 (1983); A. Garcia, Phys. Rev. D **25**, 1348 (1982).
[13]J. S. Dworkin, Ph.D. thesis, University of Michigan, 1983.
[14]J. S. Dworkin *et al.*, Nucl. Instrum. Methods **A247**, 412 (1986).
[15]Particle Data Group, M. Aguilar-Benitez *et al.*, Phys. Lett. B **170**, 1 (1986).
[16]L. Carson, R. Oakes, and C. Willcox, Phys. Rev. D **38**, 2056 (1988). We have multiplied the value for their Table VII by $M_\Lambda/(M_\Lambda+M_p)$ to be consistent with the standard notation used by experimenters.
[17]A. Sirlin, Nucl. Phys. **B161**, 301 (1979). The value of g_w is given in Eq. (19b). New measurements of the magnetic moments (see Ref. 15) have changed the predicted magnitude of g_w from 2.12 to 1.72. The value of $g_w(0)/g_v(0)$ has been obtained by setting $g_v(0)=\sqrt{3/2}$ and again multiplying by $M_\Lambda/(M_\Lambda+M_p)$.
[18]Ø. Lie-Svendsen and H. Høgaasen, Z. Phys. C **35**, 239 (1987); J. O. Eeg, H. Høgaasen, and Ø. Lie-Svendsen, *ibid.* **31**, 443 (1986). Their value has been modified because of the q^2 dependence and is given in Table VII of Ref. 16. The quoted value is obtained by multiplying by $M_\Lambda/(M_\Lambda+M_p)$.
[19]H. W. Siebert, in *Weak and Electromagnetic Interactions in Nuclei,* proceedings of the International Symposium, Heidelberg, West Germany, 1986, edited by H. V. Klapdor

(Springer, New York, 1987), p. 562.
[20]E. Klemt *et al.*, Z. Phys. C **37**, 179 (1988).
[21]J. Last *et al.*, Phys. Rev. Lett. **60**, 995 (1988).
[22]S. Y. Hsueh *et al.*, Phys. Rev. D **38**, 2056 (1988). The final value for the axial-vector-to-vector coupling-constant ratio for Σ^- β decay is $g_a(0)/g_v(0)=-0.328\pm0.019$. When this value is combined with the old world average -0.362 ± 0.043 (see Ref. 15) the result is -0.334 ± 0.017.